HHS Public Access

Author manuscript

Cell Metab. Author manuscript; available in PMC 2023 February 01.

Published in final edited form as:

Cell Metab. 2022 February 01; 34(2): 299–316.e6. doi:10.1016/j.cmet.2021.12.019.

Erythrocyte transglutaminase-2 combats hypoxia and chronic kidney disease by promoting oxygen delivery and carnitine homeostasis

Ping Xu[1,2,#], **Changhan Chen**[3,4], **Yujin Zhang**[1], **Monika Dzieciatkowska**[3], **Benjamin C. Brown**[3], **Weiru Zhang**[5], **TingTing Xie**[5], **Osheiza Abdulmalik**[6], **Anren Song**[1], **Chao Tong**[2], **Hongbo Qi**[2], **Robert Roach**[7], **Rodney E. Kellems**[1], **Angelo D'Alessandro**[3], **Yang Xia**[1,*,#]

[1]Department of Biochemistry and Molecular Biology, The University of Texas McGovern Medical School at Houston, Houston, TX, 77030, USA.

[2]Department of Obstetrics, The First Affiliated Hospital of Chongqing Medical University, Chongqing 400016, China

[3]Department of Biochemistry and Molecular Genetics, University of Colorado School of Medicine, Aurora, CO, 80045, USA.

[4]Department of Otolaryngology Head and Neck Surgery, Central South University, Changsha, Hunan, 410008, China.

[5]Department of General Medicine, Xiangya Hospital, Central South University, Changsha, Hunan, 410008, China.

[6]Division of Hematology, The Children's Hospital of Philadelphia, Philadelphia, PA 19104, USA.

[7]Altitude Research Center, Department of Emergency Medicine, University of Colorado School of Medicine, Aurora, CO, 80045, USA.

Summary

Due to lack of nuclei and de novo protein synthesis, post-translational modification (PTM) is imperative for erythrocytes to regulate oxygen (O_2) delivery and combat tissue hypoxia. Here we report that erythrocyte transglutminase-2 (eTG2)-mediated PTM is essential to trigger O_2 delivery

*Correspondence: Yang Xia. yang.xia@uth.tmc.ed.
#Lead contact: yang.xia@uth.tmc.edu

Author contributions

PX designed and conducted the mouse experiments and human sample measurements, analyzed the experimental data, drew the figures and wrote the manuscript; CC performed *in vivo* isotopically labelled glucose flux and metabolomics analysis; YZ performed CD71 isolation and mRNA analysis of BPGM; MD performed proteomics; BB and WZ conducted metabolomics; TX and MM performed P50 measurements for hypoxia-exposed mice; AS helped with trouble shooting the IP, 2,3-BPG and BPGM measurement methods; CT and HBQ provided resources for the study of primary kidney organ cultures; RR provided human high altitude samples and expertise in hypoxia; REK provided expertise in hypoxia, TG2 and proofreading the manuscript; AD provided expertise in metabolomics design and analyses and proofreading the manuscript; YX oversaw the design of experiments and interpretation of results, the writing and organization of the manuscript and did final editing.

Declaration of interests

The authors declare no competing interests.

by promoting bisphosphoglycerate mutase proteostasis and the Rapoport-Luebering glycolytic shunt for adaptation to hypoxia, in healthy humans ascending to high altitude and in two distinct murine models of hypoxia. In a pathological hypoxia model with chronic kidney disease (CKD), eTG2 is critical to combat renal hypoxia-induced reduction of *Slc22a5* transcription and OCNT2 protein levels via HIF-1α-PPARα signaling to maintain carnitine homeostasis. Carnitine supplementation is an effective and safe therapeutic approach to counteract hypertension and progression of CKD by enhancing erythrocyte O_2 delivery. Altogether, we reveal eTG2 as an erythrocyte protein stabilizer orchestrating O_2 delivery and tissue adaptive metabolic reprogramming and identify carnitine-based therapy to mitigate hypoxia and CKD progression.

eTOC blurb

Xu et al. define erythrocyte transglutminase-2 (eTG2) as a master regulator of oxygen (O_2) delivery by promoting bisphosphoglycerate mutase (BPGM) proteostasis to counteract tissue hypoxia and maintain carnitine-dependent metabolic reprogramming by inhibiting HIF-1α-PPARα axis-mediated reduction of renal *Slc22a5* transcription. Carnitine supplementation mitigates hypertension and CKD by enhancing O_2 delivery.

Graphical Abstract

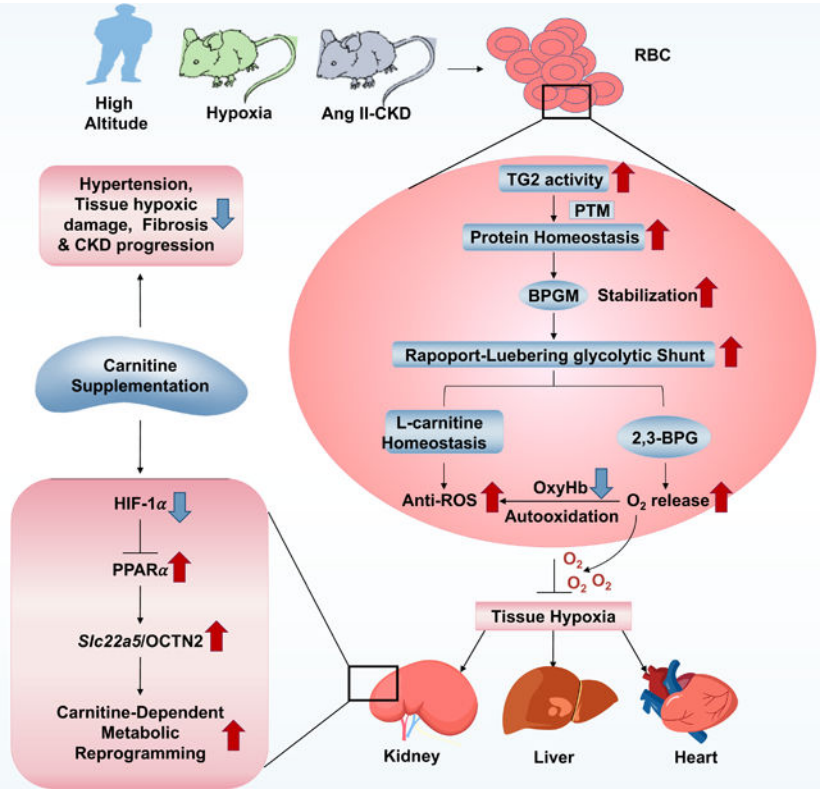

Keywords

erythrocyte; hypoxia; oxygen; transglutaminase 2; bisphosphoglycerate mutase; L-carnitine; metabolic reprogramming; proteostasis; *Slc22a5* ; organic cation/carnitine transporter 2 (OCTN2); HIF-1α; PPARα; chronic kidney disease

Introduction

Hypoxia is the central challenge to healthy individuals when they ascend to high altitude (Bärtsch and Gibbs, 2007; Hackett and Roach, 2001; Luks et al., 2008; West, 2004) and plays a pivotal role in hypoxic tissue damage and progression of almost all human diseases including chronic kidney disease (CKD), cardiovascular disease, neurodegenerative disease, chronic pulmonary obstructive disease, hemolytic disorders, trauma, hemorrhage(D'Alessandro et al., 2017) and even cancer(Arce, 2017; Basnyat, 2013; Bernauer et al., 2021; Fu et al., 2016; Semenza, 2014; Voit and Sankaran, 2020). Currently, substantial effort and research have largely focused on hypoxic damage and dysfunction of end organs. Hypoxia inducible factor (HIF) is considered a master regulator of human adaptation to high altitude and hypoxic disease pathobiology(Hammarlund et al., 2020; Lee et al., 2020). As the most abundant and only cell delivering oxygen (O_2), erythrocytes play a vital role to maintain bioenergetics and survival of every organ. To adapt to hypoxia, erythrocytes transport more O_2 to peripheral tissues to maintain tissue function and survival(Lenfant et al., 1968). Because erythrocytes lack nuclei, HIF-mediated transcriptional control and ongoing de novo protein synthesis, they rely on posttranslational modifications (PTMs) for adaptive metabolic responses that regulate O_2 off-loading to improve tissue oxygenation in the face of hypoxia(Lewis et al., 2009; Liu et al., 2016; Rogers et al., 2013; Sun et al., 2016). However, how PTMs affect erythrocyte protein homeostasis and in turn control peripheral tissue metabolic reprogramming for adaptation to hypoxia in health and disease remains poorly understood.

Notably, transglutaminase 2 (TG2) catalyzes the PTM of proteins by forming intra- or inter-protein covalent bonds between the ε-amino group of lysine and γ-carboxamide group of peptide-bound glutamine(Fesus and Piacentini, 2002). TG2 is involved in the regulation of a wide range of cellular functions and implicated to have roles in the pathogenesis of numerous diseases(Eckert et al., 2014; Iismaa et al., 2009). Although it has been known for over 30 years that TG2 is highly enriched in erythrocytes (eTG2)(Bergamini, 1988) and that TG2 gene expression is activated by HIF-1α in nucleated cells(Jang et al., 2010), nothing is known about the function of TG2 in response to hypoxia in enucleated erythrocytes under health and disease conditions.

Here, given the vital role of erythrocytes in O_2 delivery throughout the body, we sought to capture the function, metabolic and molecular events of erythrocyte TG2 (eTG2) in humans and mice with a goal to identify new therapeutics to increase tissue oxygenation and slow hypoxia-driven disease progression.

Results

eTG2 activity correlates with elevated bisphosphoglycerate mutase (BPGM) activity and carries out PTM of BPGM in healthy humans ascending to high altitude

Recent studies demonstrated that the increased erythrocyte O_2 offload in the face of hypoxia is mediated by adaptive hypoxic metabolic reprogramming that results in the activation of BPGM, a key rate limiting enzyme of the erythroid specific Rapoport-Luebering glycolytic Shunt (RLS) to generate 2,3-BPG(Liu et al., 2016; Sun et al., 2016), a negative allosteric modulator decreasing O_2 and hemoglobin (Hb) binding affinity. Thus, to determine if eTG2 is involved in hypoxia-induced metabolic adaptation, we carried out human high-altitude studies and chose to quantify the activity of eTG2 and its relationship to hypoxia-induced BPGM activity, 2,3-BPG levels and P50 in young healthy human volunteers participating in the AltitudeOmics study(Subudhi et al., 2014) (Table S1). We found that eTG2 activity was induced by high altitude hypoxia along with activation of BPGM, elevated 2,3-BPG and increased P50 (defined as the partial pressure of O_2 required for 50% hemoglobin binding to O_2), indicating O_2 releasing capacity was increased in the erythrocytes of both males and females in a time-dependent manner (Figure 1a). Moreover, we found that not only 2,3-BPG and P50 were correlated, but also eTG2 activation was positively correlated with elevated BPGM activity (Figure 1a).

Next, we used an antibody that specifically recognizes lysine-glutamine isopeptide bonds to determine whether increased TG2 activity upon exposure to high altitude leads to TG2-catalyzed PTM(Mi et al., 2017). Consistent with the increased eTG2 activity, a similar time-dependent increase in lysine-glutamine isopeptide bond formation in erythrocytes was observed in humans ascending to high altitude from day 1 until day 16 (Figure 1b). Particularly, we showed that elevated erythrocyte TG2 catalyzed the PTM of BPGM by forming intra-protein covalent bonds between lysine and γ-carboxamide groups of peptide-bound glutamines in response to high altitude without an effect on BPGM protein levels (Figure 1b). Thus, eTG2 activity is rapidly induced by hypoxia, TG2 activity positively correlates with elevations in BPGM activity, and the level of isopeptide bonds – a TG2-catalyzed reaction – increases in BPGM following ascent to high-altitude.

Ablation of eTG2 abolishes hypoxia-induced BPGM activation and O_2 delivery

To determine the role of eTG2 in hypoxia metabolic adaptation, we generated erythrocyte-specific TG2 knockouts by mating mice with floxed TG2 alleles (*Tgm2*$^{f/f}$) with mice containing a transgene expressing Cre recombinase only in the erythroid lineage (*EpoR-Cre*$^{+}$)(Heinrich et al., 2004) (Figure S1a-S1c). The *Tgm*$^{f/f}$*EpoR-Cre*$^{+}$ mice are fertile and morphologically indistinguishable from littermates through adulthood. First of all, to validate that BPGM is modified by eTG2 in mice as seen in humans (Figure 1b), we performed pull-down experiments with isopeptide-specific antibodies followed by proteomics in erythrocytes purified from *Tgm2*$^{f/f}$*EpoR-Cre*$^{+}$ and *EpoR-Cre*$^{+}$ mice under normoxia. Proteomics analyses identified 23 candidate protein targets of eTG2 in mouse RBCs, including proteins involved in metabolism, cellular processes and adhesion (Figure S2a & S2b). Importantly, proteomics confirmed that BPGM is a target of eTG2 in mouse erythrocytes at normoxia (75% sequence coverage - Figure S2c).

Next, to mimic human high-altitude studies, we exposed *Tgm2$^{f/f}$EpoR-Cre^{+}* mice and *EpoR-Cre^{+}* mice to hypoxia (10% O_2) for 48 hours (Figure 1c). Similar to humans in the AltitudeOmics study, hypoxia significantly induced eTG2 and BPGM activity as well as P50 in erythrocytes of *EpoR-Cre^{+}* control mice, while loss of eTG2 abolished hypoxia-induced BPGM activation and P50 (Figure 1c). Thus, we conclude that eTG2 is required for hypoxia-induced BPGM activation and O_2 delivery in mice.

eTG2-mediated PTM promotes BPGM proteostasis vs proteolysis

To probe the molecular basis underlying eTG2-mediated hypoxia-induced activation of BPGM, we compared erythrocyte BPGM protein levels between controls and *Tgm2$^{f/f}$EpoR-Cre^{+}* mice under normoxia and hypoxia. Similar to the human studies, hypoxia did not alter erythrocyte BPGM protein levels in control mice (Figure 1d-e). Surprisingly, however, loss of eTG2 decreased the amount of BPGM protein to about half normal levels under both normoxia and hypoxia compared to the *EpoR-Cre^{+}* controls (Figure 1d-e). Although *Tgm2$^{f/f}$EpoR-Cre^{+}* mice have half the amount of BPGM protein, they maintain a normal level of BPGM activity as the controls under normoxia. However, the reduced amount of BPGM protein in *Tgm2$^{f/f}$EpoR-Cre^{+}* mice cannot be further activated by the challenge of hypoxia. These findings rule out the possibility that TG2-mediated PTM directly induces BPGM activity, but strongly support the possibility that eTG2-mediated PTM is essential to maintain BPGM proteostasis. As such, increased TG2 activity under hypoxia is critical to stabilize BPGM protein levels and prevent its loss in both humans ascending to high altitude (Figure 1a) and control mice (Figure 1c) exposed to hypoxia.

Next, to determine if the reduced BPGM protein level in *Tgm2$^{f/f}$EpoR-Cre^{+}* mice is mediated by decreased transcription at an early erythroid stage, we compared BPGM mRNA in isolated $CD71^{+}$ erythroblasts between controls and *Tgm2$^{f/f}$EpoR-Cre^{+}* mice under normoxia. No difference in BPGM mRNA levels was found in isolated $CD71^{+}$ erythroblasts between controls and *Tgm2$^{f/f}$EpoR-Cre^{+}* mice under normoxia, ruling out the possibility that downregulation of BPGM protein levels in *Tgm2$^{f/f}$EpoR-Cre^{+}* mice is due to reduced BPGM gene transcription at an early stage in the erythroid lineage (Figure S1d). Thus, our findings implicate that TG2 controls BPGM proteostasis vs proteolysis and maintains BPGM homeostasis. Intriguingly, we found that erythrocyte ubiquitinated proteins were slightly induced by hypoxia in the control mice and humans (Figure 1f) along with elevated TG2 activity (Figure 1a,1c). However, erythrocyte polyubiquitinated proteins were significantly higher in *Tgm2$^{f/f}$EpoR-Cre^{+}* mice than the controls under normoxia and further induced in *Tgm2$^{f/f}$EpoR-Cre^{+}* mice under hypoxia (Figure 1f), suggesting that TG2 interferes with polyubiquitination and in turn stabilizes erythrocyte proteins and maintains protein homeostasis both in human and mice facing hypoxia.

TG2-mediated PTM stabilizes erythrocyte BPGM and maintains protein homeostasis by competing against polyubiquitination and degradation.

In addition to forming isopeptide bonds by transamination, TG2 is reported to be a guanine nucleotide signaling protein(Nakaoka et al., 1994), a kinase(Mishra et al., 2006), a protein disulfide isomerase(Hasegawa et al., 2003) and a scaffolding factor(Akimov et al., 2000). Protein ubiquitination forms a glycine-lysine bond between ubiquitin and its

acceptor, whereas TG2-mediated PTM forms a glutamine-lysine isopeptide bond(Hershko et al., 2000; Komander and Rape, 2012). Thus, we hypothesized that eTG2-mediated transamination directly inhibits polyubiquitin conjugations and in turn stabilizes proteins. To address this possibility, we treated purified human erythrocytes with cystamine, a specific inhibitor of transglutaminase(Siegel and Khosla, 2007) (Figure 2a). Cystamine treatment successfully inhibited TG2 activity in a dose and time-dependent manner (Figure 2b). Like the *in vivo* studies with mice carrying a genetic ablation of eTG2 (Figure 1f), pharmacological inhibition of eTG2 activity via cystamine treatment induced RBC protein polyubiquitination and subsequent degradation of BPGM in a dose and timedependent manner (Figure 2c). Next, we conducted co-immunoprecipitation (co-IP) experiments using antibodies specific for the Nε-(γ-glutamyl)-lysine isopeptide bond, ubiquitin or BPGM followed by western blot analysis to probe the specific effects of cystamine on isopeptide modification and polyubiquitination conjugation on BPGM. Isopeptide modification of BPGM was reduced by cystamine treatment, whereas polyubiquitination of BPGM was increased (Figure 2d). Similar results were seen with cultured mouse RBCs (Figure 2e-2g). Altogether, we revealed that eTG2-mediated PTM controls proteostasis by interfering with polyubiquitination and proteolysis in erythrocytes, in particular for BPGM.

eTG2-mediated BPGM proteostasis promotes erythrocyte metabolic reprogramming and O_2 offload in hypoxia-driven CKD

The importance of eTG2 in physiological hypoxia immediately suggests its essential role in combating pathological hypoxia, a major driving force for numerous diseases(Ientile et al., 2007). Thus, to explore the role of eTG2 in hypoxia-driven disease progression, we chose a well-established experimental model of chronic kidney disease (CKD) based on infusion with angiotensin II (Ang II), a potent vasoconstrictor(Forrester et al., 2018; Xie et al., 2020b). Similar to physiological hypoxia, Ang II induced eTG2 and BPGM activity in control mice, while loss of eTG2 completely abolished Ang II-induced BPGM activity in *Tgm2*$^{f/f}$*EpoR-Cre*$^{+}$ mice (Figure 3a). Total polyubiquitinated protein levels were substantially induced, while isopeptide modified protein levels were significantly reduced in Ang II-infused *Tgm2*$^{f/f}$*EpoR-Cre*$^{+}$ mice compared to controls (Figure 3b & Figure S3a). Similar to hypoxia, basal BPGM protein levels were reduced by half in *Tgm2*$^{f/f}$*EpoR-Cre*$^{+}$ mice independent of Ang II infusion (Figure 3b & Figure S3a). Unlike BPGM, loss of eTG2 did not affect the protein levels of GAPDH and G6PD, enzymes involved in glycolysis and pentose phosphate pathway (PPP), respectively (Figure 3b & Figure S3a). Thus, eTG2-mediated PTM is essential to stabilize BPGM protein and in turn promote Ang II-induced BPGM activity.

To gain a comprehensive understanding of how eTG2 controls erythrocyte metabolism, we performed metabolomics analyses of purified mature erythrocytes from control and *Tgm2*$^{f/f}$*EpoR-Cre*$^{+}$ mice with and without Ang II infusion. A total of 299 metabolites were identified in the purified mouse erythrocytes (Table S3). Among the metabolic pathways examined, glycolysis and RLS intermediates including 2,3-BPG were significantly affected in *Tgm2*$^{f/f}$*EpoR-Cre*$^{+}$ mice with Ang II infusion compared to the controls (Figure 3c). We validated our metabolomic analysis by performing additional targeted quantitative analysis of 2,3-BPG (Figure 3d). Functionally, Ang II induced P50 in the control mice but not the

mutant mice (Figure 3d). Additional *in vivo* tracing experiments with [1,2,3]-$^{13}C_3$-glucose allowed us to confirm significant increases in fluxes through glycolysis and RLS vs PPP, leading to increased 2,3-BPG production in *EpoR-Cre*$^{+}$ mice, but not in *Tgm2*$^{f/f}$*EpoR-Cre*$^{+}$ mice following Ang II infusion (full list of labeled isotopologue intermediates for these pathways is shown in Figure 3e). Although the first product of the PPP (6PGL) was not induced by Ang II in eTG2-deficient mice, S7P, one of the important downstream metabolites of 6PGL in the PPP was significantly induced in mutant mice (Figure 3e), implicating that the PPP is increased and rapidly converts 6PGL to S7P in eTG2 mutants. Supporting this possibility, lactate (M2+), the end product generated from 6PGL in the PPP, was significantly higher in mutant mice than the controls with Ang II infusion (Figure 3e). Thus, despite glucose metabolism channeling toward PPP over glycolysis/RLS in eTG2-deficient mice, it is likely insufficient to counteract overwhelming oxidative stress generated by autooxidation of the oxyhemoglobin (oxyHb) that accumulates because of reduced 2,3-BPG. Supporting this possibility, Ang II infusion led to a significantly higher amount of reactive oxygen species (ROS) and a substantial higher ratio of GSSG/GSH in the mutants than the controls (Figure 3d). Altogether, eTG2 catalyzes isopeptide bond formation and inhibits polyubiquitin-conjugation, in turn stabilizes BPGM protein level, enhances glucose metabolism toward glycolysis-RLS instead of PPP to induce 2,3-BPG production and promote O_2 release. After O_2 (the source of oxidative stress) is released from oxyHb, the oxidative stress generated by autooxidization of oxyHb is reduced and thus the demand for antioxidants generated by PPP in erythrocytes is reduced. (Figure 3f).

eTG2 is required for L-carnitine-dependent renal metabolic reprogramming in CKD

Systemically, loss of eTG2 did not affect Ang II-induced hypertension (Figure 4a). However, impaired erythrocyte O_2 release in Ang II-infused *Tgm2*$^{f/f}$*EpoR-Cre*$^{+}$ mice compared to the controls aggravated renal hypoxia, kidney damage and fibrosis. Specifically, renal injury score, proteinuria, plasma urea and creatinine, tissue fibrosis measured by Masson's trichrome staining and the expression of fibrotic marker genes such as fibronectin (FN) and collagens (Col1a1, Col3a1and Col4a1) were significantly elevated in Ang II-infused *Tgm2*$^{f/f}$*EpoR-Cre*$^{+}$ mice compared to the controls (Figure 4b-4d & Figure S4a). In addition to kidneys, severe hypoxia and fibrosis were also induced in heart and liver of Ang II-infused *Tgm2*$^{f/f}$ *EpoR-Cre*$^{+}$ mice compared to the controls (Figure 4c), indicating that erythrocyte TG2 is required to combat chronic Ang II-induced tissue hypoxia, damage and fibrosis.

Next, we determined whether eTG2 deficiency has any impact on the local renal RAS in the Ang II-induced CKD model. We found no significant differences in the renal mRNA levels of RAS components between EpoR-Cre^{+} and *Tgm2*$^{f/f}$*EpoR-Cre*$^{+}$ mice with or without Ang II treatment (Figure S4d). Thus, our studies provide proof-of-principle genetic evidence that TG2-mediated PTM is critical to maintain BPGM proteostability, 2,3-BPG production and O_2 release from erythrocytes to increase renal oxygenation and reduce kidney damage, renal dysfunction and progression to CKD independent of hypertension and local RAS-mediated renal vasoconstriction.

Kidney is the major organ that produces erythropoietin and CKD is associated with anemia(Voit and Sankaran, 2020). Ang II is a growth factor for erythroid progenitors in cooperation with erythropoietin. However, a complete blood count showed no significant differences in erythrocyte numbers and Hb concentration between *Tgm2*$^{f/f}$*EpoR-Cre*$^{+}$ mice and controls with or without Ang II infusion (Figure S4b), ruling out the possibility that the severe CKD phenotype observed in *Tgm2*$^{f/f}$*EpoR-Cre*$^{+}$ mice is due to decreased erythropoiesis. Thus, consistent with human and mouse studies under physiological hypoxia, in this Ang II-induced model of CKD we confirmed that eTG2-mediated modification of BPGM promotes proteostasis vs proteolysis, controls erythrocyte metabolic reprograming-induced 2,3-BPG production and O_2 delivery and thus attenuates hypoxia-driven disease progression.

We set out to identify the metabolic basis underlying severe tissue hypoxia, damage and disease progression seen in our model of CKD in eTG2-deficient mice. To this end, we conducted untargeted metabolomics in plasma, kidney and urine in addition to erythrocytes from controls and *Tgm2*$^{f/f}$*EpoR-Cre*$^{+}$ mice following saline or Ang II infusion (Figure 4e & Table S3). *Tgm2*$^{f/f}$*EpoR-Cre*$^{+}$ mice infused with AngII were characterized by an insufficient O_2 supply, increased renal glycolysis and decreased TCA cycle (Figure 4f). Consistent with the metabolic data, renal mRNA levels of several glycolytic enzymes, such as hexokinase (HK), pyruvate kinase (PK) and lactate dehydrogenase 2 (LDH2) were induced in mutant mice (Figure S4c). Unexpectedly, the most significantly and commonly reduced metabolites among kidney, plasma and erythrocytes are L-carnitine and acyl-carnitines in Ang II-infused *Tgm2*$^{f/f}$*EpoR-Cre*$^{+}$ mice compared to the controls (Figure 4f & Figure S4e). In contrast, urine metabolomics revealed that the L-carnitine levels were increased in the mutant mice with Ang II infusion in a time-dependent manner (Figure 4g). L-carnitine is a rate-limiting substrate to generate acyl-carnitines, both for fatty acid transport into mitochondria for O_2-dependent fatty acid oxidation and energy production and for the preservation of lipid homeostasis in equilibrium with acyl-CoA counterparts, as part of damage repair mechanisms such as the Lands' cycle(El-Hattab and Scaglia, 2015). L-carnitine is mainly obtained from the diet and a small portion is synthesized endogenously. Kidneys play a role in carnitine biosynthesis from lysine and methionine(Guder and Wagner, 1990). Metabolomics showed that neither lysine nor methionine levels were reduced (Figure S4f), ruling out impaired renal carnitine biosynthesis.

L-carnitine is excreted from the kidney and an organic cation/carnitine transporter 2 (OCTN2)(Wu et al., 1999), is involved in tubular reabsorption of filtered carnitine. In view of our findings that L-carnitine levels were increased in the urine but decreased in kidney, erythrocytes and plasma in Ang II-infused mutant mice, it is possible that increased renal excretion of L-carnitine is associated with impaired L-carnitine reabsorption. Supporting this possibility, OCTN2 protein and *Slc22a5* (the gene encoding OCTN2) mRNA levels were significantly reduced in the kidneys of Ang II-infused *Tgm2*$^{f/f}$*EpoR-Cre*$^{+}$ mice compared to controls (Figure 4h & Figure S4g). Unlike kidneys, there were no differences in OCTN2 protein levels in erythrocytes between mutants and controls with or without Ang II infusion (Figure 4h & Figure S4g). Thus, our studies raise an intriguing and compelling hypothesis that eTG2 ablation leads to downregulation of renal OCTN protein levels, decreased renal

reabsorption of L-carnitine and increased loss to the urine, resulting in impaired L-carnitine-dependent metabolic reprogramming.

L-carnitine supplementation improves tissue oxygenation and combats progression of CKD.

To test above hypothesis and determine if L-carnitine is an effective and safe treatment for CKD, we treated Ang II infused control and *Tgm2*$^{f/f}$*EpoR-Cre*$^{+}$ mice with supplementary L-carnitine from Day 7 to Day 21 (as the increased L-carnitine in urine was observed on Day 7, Figure 4g) and harvested samples on Day 21 for analyses (Figure 5a). L-carnitine supplementation rescued the Ang II-induced severe CKD phenotype in eTG2 knockouts and attenuated CKD development in control mice by reducing hypertension and tissue hypoxia and slowing down the kidney damage and the progression to fibrosis (Figure 5b-5f). Moreover, L-carnitine supplementation significantly lowered ROS levels in the erythrocytes of both controls and *Tgm2*$^{f/f}$*EpoR-Cre*$^{+}$ mice infused with Ang II (Figure 5g). L-carnitine had no obvious effect on either 2,3-BPG levels or BPGM activity in either Ang II-infused controls or *Tgm2*$^{f/f}$*EpoR-Cre*$^{+}$ mice. Instead, L-carnitine significantly increased erythrocyte ATP levels in Ang II-infused *Tgm2*$^{f/f}$*EpoR-Cre*$^{+}$ mice (Figure 5g). Like 2,3-BPG, ATP can bind to Hb and lower Hb-O_2 binding affinity to enhance O_2 delivery(Benesch and Benesch, 1969; Ellsworth et al., 2009). As such, L-carnitine restored erythrocyte O_2 delivery capacity of Ang II-infused *Tgm2*$^{f/f}$*EpoR-Cre*$^{+}$ mice (Figure 5g). Thus, in Ang II-infused eTG2 knockouts, L-carnitine supplementation-mediated rescue of severe CKD phenotype is due to dual therapeutic effects including anti-hypertension-mediated enhanced blood flow to kidneys and improved O_2 delivery and decreased ROS in the erythrocytes. In Ang II-infused control mice, L-carnitine supplementation-mediated improvement of the mild CKD phenotype is largely due to anti-hypertension and anti-ROS therapeutic effects in erythrocytes. Overall, L-carnitine is an essential metabolite underlying adaptive metabolic reprogramming and has multiple therapeutic effects on both peripheral tissues and erythrocytes to combat hypoxiadriven CKD progression.

Molecular Links of eTG2-mediated enhanced erythrocyte O_2 offload in combating CKD Hypoxia-mediated downregulation of OCTN2 via HIF-1α-PPARα axis inking eTG2 ablation to Ang II-induced carnitine loss, renal damage and severe CKD

Our preclinical studies described above demonstrate that decreased *Slc22a5* (the gene encoding OCTN2) mRNA and OCTN2 protein resulted in excess urinary carnitine loss, a central pathogenic feature of CKD in eTG2 knockouts. However, how eTG2 ablation is linked to decreased renal *Slc22a5* transcription and reduced OCTN2 protein remained unknown. Severe hypoxia, renal damage and the CKD phenotype that developed in Ang II-infused eTG2 knockouts are not due to either hypertension or elevated local renal RAS-mediated vasoconstriction. Realizing that HIF-1α is a master transcription factor induced by hypoxia (Iyer et al., 1998) (McGettrick and O'Neill, 2020) and that hypoxia is reported to reduce OCTN2 levels (Chang et al., 2011; Wojtal et al., 2014), we immediately considered the possibility that elevated HIF-1α underlies reduction of renal *Slc22a5* transcription and OCTN2 production in Ang II-infused eTG2-deficient mice (Figure 6a). Due to complexity of an intact animal, we chose to conduct experiments using primary mouse renal organ culture closely mimicking kidney to determine if HIF-1α functioning downstream of renal

hypoxia directly downregulates *Slc22a5* transcription independent of hypertension and renal RAS changes. We found that hypoxia exposure or treatment with HIF-1α stabilizer, dimethyloxalylglycine (DMOG), induced HIF-1α protein levels and in turn reduced *Slc22a5* mRNA and OCTN2 protein levels, while the reduction was significantly attenuated by Chrysin, a specific prolyl hydroxylase activator that promotes degradation of HIF-1α (Figure 6b-c). These findings led us to conclude that elevated HIF-1α underlies hypoxia-mediated downregulation of renal *Slc22a5* transcription.

Notably, early studies showed that PPARα directly controls transcription of *Slc225a* by binding to PPARα specific regulatory elements (Luo et al., 2014; Maeda et al., 2008; Wen et al., 2010) and that HIF-1α is known to downregulate the transcription of the PPARα gene (Narravula and Colgan, 2001). Thus, we hypothesized that HIF-1α-induced downregulation of PPARα is responsible for hypoxia-mediated reduction of renal *Slc22a5* transcription and reduced OCTN2 protein production (Figure 6d). To test this hypothesis, we cultured murine kidney organ explants challenged with hypoxia or treated with DMOG in the presence or absence of Fenofibrate, a PPARα agonist. Early studies showed that Fenofibrate not only functions as PPARα agonist, but at higher concentrations also induces transcription of PPARα gene and increases its protein production (Hsu et al., 2020; Rahman et al., 2009). Consistent with these earlier results, we found that Fenofibrate significantly induced both mRNA and protein levels of PPARα at higher concentrations (Figure 6e). As such, Fenofibrate significantly attenuated hypoxia or DMOG-induced reduction in *Slc22a5* mRNA and OCTN2 protein levels in a dosage-dependent manner (Figure 6e). Thus, we identified that the HIF-1α-PPARα signaling axis underlies hypoxia-mediated reduction in renal *Slc22a5* transcription (Figure 6f).

Similar to the *in vitro* kidney organ culture exposed to hypoxia, we demonstrated that renal HIF-1α levels were significantly induced, while PPARα and OCTN2 proteins and *Slc22a5* mRNA levels were significantly reduced as a result of the severe renal hypoxia in Ang II-infused eTG2-deficient mice (Figure 7b-7c). However, Ang II infusion in control mice only induced mild renal hypoxia and mild CKD, which was insufficient to cause HIF-1α–PPARα axis-mediated reduction of *Slc22a5* transcription in control mice (Figure 7b-7c). Taken together, we provide both *in vitro* and *in vivo* evidence that severe hypoxia signaling via HIF-1α-PPARα axis-mediated reduction of renal *Slc22a5* mRNA and OCTN2 protein levels and subsequent impairment of renal carnitine reabsorption function as a positive feedforward loop to promote excess carnitine loss and the progression of CKD in Ang II-infused eTG2 knockouts (Figure 6f). Thus, eTG2 is critical to combat urinary carnitine loss, promote carnitine-dependent metabolic reprogramming and attenuate severe CKD development by enhancing erythrocyte O_2 offload and mitigating HIF-1α-PPARα axis-mediated reduction of OCTN2.

Restoration of hypoxia-mediated HIF-1α-PPARα-dependent downregulation of renal *Slc22a5* transcription underlies the improvement in CKD by carnitine supplementation in Ang II-infused *eTG2*$^{-/-}$ mice

L-carnitine supplementation rescued the severe hypoxia and CKD phenotype in eTG2-deficient mice largely due to reduced hypertension and enhanced O_2 delivery capacity

from erythrocytes (Figure 5b-5f). Thus, we hypothesize that the improvement in CKD by carnitine supplementation is associated with attenuated renal hypoxia-mediated elevation of HIF-1α, allowing restoration of PPARα-mediated *Slc22a5* transcription in Ang II-infused eTG2 deficient mice (Figure 7a). Supporting this possibility, we found that carnitine supplementation significantly restored renal PPARα and OCTN2 protein and mRNA levels along with reduced renal HIF-1α protein levels in Ang II-infused eTG2 deficient mice (Figure 7b-c). This finding led us to conclude that L-carnitine treatment attenuated severe renal hypoxia-mediated elevated HIF-1α and restored renal *Slc225a* mRNA and OCTN2 protein levels via enhanced PPARα signaling and is a key mechanism underlying the improved CKD phenotype in eTG2-deficient mice.

To determine if carnitine can directly attenuate hypoxia-induced reduction of renal OCTN2, we exposed primary kidney organ cultures to hypoxia or DMOG in the presence or absence of L-carnitine. We found that L-carnitine treatment had no effect on either OCTN2 protein levels, *Slc22a5* mRNA levels or HIF-1α-PPARα expression in primary kidney organ cultures under hypoxia (Figure 7d & Figure S5a-b)or with DMOG-treatment (Figure 7e & Figure S5a-b). These finding rule out the possibility that L-carnitine treatment has a direct effect on the hypoxia-mediated HIF-1α-PPARα-dependent downregulation of renal *Slc22a5* transcription.

Overall, both *in vivo* and *in vitro* studies allow us to identify that L-carnitine treatment improved erythrocyte O_2 delivery and attenuated hypertension as dual therapeutic effects mitigating severe renal hypoxia-mediated reduced OCTN2 production via HIF-1α-PPARα signaling, a key mechanism underlying rescue of the severe CKD phenotype in eTG2-deficient mice. In Ang II-infused control mice, L-carnitine mediated attenuation of the mild CKD phenotype is largely due to anti-hypertensive and anti-ROS therapeutic effects in erythrocytes without the impact of HIF-1α-PPARα-mediated reduction of *Slc22a5* mRNA and OCTN2 protein levels (Figure 7e)

Discussion

In conclusion, we report major unexpected discoveries showing that eTG2 is beneficial to induce tissue adaptive hypoxic metabolic reprogramming by acting as an erythrocyte critical “protein stabilizer”, “metabolic reprogrammer” and “O_2 delivery facilitator” to combat both physiological and pathological hypoxia in humans and mice. Additionally, we identified carnitine-based therapy to increase tissue oxygenation and slow hypoxia-driven CKD progression.

Unique among cells, enucleated erythrocytes have no ability to synthesize new proteins, but retain a functional ubiquitin proteasomal system (UPS)(Kakhniashvili et al., 2004). Hypoxia promotes the UPS in erythrocytes(Song et al., 2017). However, once a protein is degraded by the UPS it is permanently lost due to the lack of ongoing transcription and translation. Thus, “defensive” mechanisms controlling proteostasis versus proteolysis are extremely critical in erythrocytes. However, very little is understood about how erythrocytes properly maintain protein homeostasis under health and disease, in particular when facing hypoxia. Here we report that eTG2 plays a key mechanistic role in erythrocyte proteostasis,

metabolism and function to combat physiological and pathological hypoxia. Specifically, we revealed that eTG2-mediated PTM is critical to prevent polyubiquitination and in turn selectively stabilize specific erythrocyte proteins to maintain protein homeostasis. Our proteomics data identified 23 potential TG2-modified substrates. Pathway analysis indicates that those identified protein candidates are important in metabolism, adhesion, locomotion and cellular structure. For example, Flotillin-2 (Flot2) and Gamma-adducin (Add3) are prominent components of the erythrocyte membrane and involved in lipid raft formation (Biernatowska et al., 2017; Robledo et al., 2010). Among identified targets we provided both genetic proof-of-principle and pharmacological *in vitro* evidence showing that eTG2-mediated PTM is essential to maintain BPGM proteostasis by interfering with polyubiquitination and subsequent proteolysis. As such, increased eTG2 activity is a critical adaptive hypoxic response to stabilize BPGM protein levels and eventually enhancing O_2 offloading from erythrocytes in both humans ascending to high altitude and mice challenged with hypoxia or CKD. Notably, earlier studies showed increased BPGM activity, 2,3-BPG levels and P50 in CKD patients (Xie et al., 2020a). Thus, it is important to validate if elevated eTG2-mediated BPGM proteostasis contributes to its activation, 2,3-BPG induction and enhanced O_2 offload in CKD patients. Additionally, carbamylation is a non-enzymatic and irreversible PTM resulting from interaction between isocyanic acid and amino groups of proteins. Carbamylation can modify lysine residues of polypeptide chains to generate an ε-carbamyl-lysine bond (*i.e.*, homocitrulline). Given the fact that increased carbamylation is reported in CKD (Berg et al., 2013) and end-stage renal disease (Berg et al., 2013) due to elevated urea, the toxic end product of protein catabolism and a precursor of isocyanic acid, and that TG2 catalyzes covalent bond-formation between the ε-amino group of lysine and γ–carboxamide group of peptide-bound glutamine, it will be interesting to see whether TG2 activation affects carbamylation in erythrocytes of CKD patients.

Interestingly, although ablation of eTG2 reduces BPGM protein levels by 50%, it has no impact on the basal level of BPGM activity and O_2 offload but only abolishes the enhanced BPGM activation and O_2 delivery capacity facing the challenge of hypoxia and CKD. These findings implicate that there is a TG2-independent mechanism responsible for maintaining a normal level of BPGM activity and O_2 offloading in eTG2-deficient mice under normoxia, while such a mechanism is lost in eTG2-deficient mice challenged with hypoxia or CKD. Notably, erythrocytes are well equipped with a sophisticated regulatory system to activate glycolytic enzymes to adapt to physiological and pathological hypoxia(D'Alessandro and Xia, 2020; Lewis et al., 2009; Low et al., 1993; Rogers et al., 2009). For example, adenosine mediated activation of the sphingosine-1-phosphate-PP2A-AMPK signaling cascade is reported to regulate BPGM activation under hypoxia (Sun et al., 2016) and CKD(Peng et al., 2019; Xie et al., 2020a). Thus, this hypoxia-sensitive signaling network is likely already activated to induce BPGM activity and O_2 offload in eTG2-deficient mice as the control mice under normoxia. However, such a compensatory adaptive response may be unable to further activate BPGM in the eTG2-deficient mice in response to challenge of hypoxia and CKD. Moreover, substantial studies reported that TG2 gene expression is regulated by hypoxia and inflammation in nucleated cells(Su et al., 2021; Zonca et al., 2017). However, how eTG2 enzyme activity is induced by hypoxia in enucleated mature erythrocytes remains unresolved. Notably, early studies showed that adenosine induces TG2 activity in H9c2

cells(Vyas et al., 2016). Given the critical role of the adenosine-sphingosine 1 phosphate-PP2A-AMPK signaling axis in erythrocyte metabolic and hypoxic adaptation by inducing BPGM activation (Xie et al., 2020b), this signaling cascade likely also controls eTG2 activation under hypoxia in mature erythrocytes. Taken together, our finding supports a new working model that eTG2-mediated PTM and the adenosine-S1P-PP2A-AMPK signaling axis are two critical components working together to promote TG2 activation, prevent BPGM proteolysis and induce BPGM activation for adaptation to both physiological and pathological hypoxia.

Erythrocytes deliver O_2 but do not use O_2. Enhanced erythrocyte O_2 delivery is vital for peripheral tissue metabolic reprogramming by fully oxidizing major nutrients to maximize energy production for survival under stress. To our knowledge, regulatory mechanisms of erythrocyte-induced tissue oxygenation and adaptive hypoxic metabolic reprogramming remain largely unknown. Here we revealed that eTG2-mediated proteostasis of BPGM and enhanced O_2 delivery counteracts tissue hypoxia, renal dysfunction, progression to CKD and enhances tissue adaptive metabolic reprogramming featured with decreased glycolysis, increased fatty acid oxidization and TCA cycle metabolism, independent of hypertension and local RAS-mediated renal vasoconstriction. L-carnitine is important for fatty acid oxidation in mitochondria(El-Hattab and Scaglia, 2015) and for the Lands' cycle to repair oxidized membrane lipids in erythrocytes(Wu et al., 2016). However, the regulation and function of eTG2 in carnitine metabolism has not been previously recognized. Here we report that carnitine emerges as an important metabolite for both erythrocyte and tissue metabolic reprogramming for hypoxia adaptation in Ang II-induced CKD. Our metabolomics led to an unexpected discovery that L-carnitine levels are decreased in kidney, erythrocytes and plasma but increased in the urine due to downregulation of renal OCTN2 levels in eTG2 knockout mice with CKD. Mechanistically, we further revealed that eTG2-deficiency resulted in renal hypoxia and the activation of a HIF-1α-PPARα signaling axis that links renal damage and progression of CKD with reduced renal *Slc22a5* transcription and the loss of urinary carnitine reabsorption. As such, insufficient O_2 and L-carnitine work together to aggravate tissue damage and dysfunction as a vicious cycle to promote disease progression. Expanding on these findings, our preclinical, interventional studies revealed that carnitine loss is a key pathology for CKD and a carnitine-based therapy may be a safe and effective treatment for hypoxia-driven CKD. Mechanistically, carnitine treatment lowers hypertension and restores enhanced erythrocyte O_2 delivery by attenuating renal hypoxia-mediated downregulation of *Slc22a5* transcription via HIF-1α-PPARα signaling. As such, carnitine supplementation led to enhanced blood flow and O_2 supply and the restoration of carnitine homeostasis to combat Ang II-induced damage and progression of CKD in eTG2-deficient mice. In contrast, eTG2-mediated stabilization of BPGM is maintained in control mice with Ang II infusion. Thus, BPGM activity, 2,3-BPG levels and O_2 offload from erythrocytes are induced in Ang II-infused control mice. As such, Ang II only induced mild hypoxia and a mild CKD phenotype without significant effects on the HIF-1α-PPARα signaling axis and downregulation of *Slc22a5* mRNAs and OCTN2 protein. Carnitine supplementation lowered ROS in erythrocytes and enhanced BPGM homeostasis to combat Ang II-induced mild CKD in control mice (Figure 7f). Supporting our findings, lower plasma carnitine(Bissinger et al., 2021; Di Liberato et al., 2014) and reduced renal

fatty acid metabolic gene expression(Kang et al., 2015) are reported in CKD patients. Moving forward, our mechanistic and preclinical studies establish a strong foundation for carnitine-based therapy in CKD patients.

PTMs such as phosphorylation and ubiquitination are widely studied and well recognized to regulate cell signaling, homeostasis and function. In contrast, TG2-mediated PTM in erythrocyte proteostasis, metabolism and function for tissue hypoxia metabolic adaption remained unrecognized prior to our studies presented here. Given the vital role of O_2 and L-carnitine in bioenergetics in almost every cell within our body, we anticipate that the newly identified signaling axis and metabolic network mediated by eTG2 could play an important role in many diseases, beyond CKD, in which hypoxia is an etiological contributor, including aging, neurodegenerative diseases, cardiovascular disease and cancer.

Limitations of the study

For the human studies, the role of eTG2-mediated PTM in promoting erythrocyte BPGM proteostasis and enhancing O_2 delivery was determined only in healthy individuals ascending to high altitude. To assess the generality of these findings it will be important to examine other cases of tissue hypoxia, including hypertensive patients with CKD. Moreover, eTG2-induced O_2 delivery to combat hypoxic tissue damage, HIF1α-PPARα signaling axis-mediated downregulation of renal *Slc22a5* transcription, urinary carnitine loss and progression of CKD was solely determined in an Ang II-infusion induced model of hypertensive CKD, making generalization to other CKD models not possible. Although eTG2-mediated PTM was found to stabilize BPGM and promote adaptive hypoxic metabolic reprogramming, the functional role of eTG2-mediated PTM on other proteins remains to be determined. eTG2 activity was induced by hypoxia or Ang II infusion. However, the specific mechanisms underlying eTG2 activation by hypoxia or Ang II were not determined and will be the focus of future studies. Owing to the effective and safe use of carnitine supplementation to treat Ang II-induced CKD in mice, it will be important to investigate the *in vivo* benefits of carnitine treatment in other hypoxic conditions such as humans ascending to high altitude and in other mouse models of pathological hypoxia. The results of such studies may show that carnitine-based therapies have broad clinical application.

STAR Methods

RESOURCE AVAILABILITY

Lead Contact—Further information and requests for resources and reagents should be directed to and will be fulfilled by the Lead Contact, Yang Xia (yang.xia@uth.tmc.edu).

Material availability—Mouse lines generated in this study are available from the lead contact upon request. This study did not generate new unique reagents.

Data and code availability

- Unprocessed data underlying the display items in the manuscript are presented in Data S1 and S2 files as supplemental material.
- This paper does not report original code.

- Any additional information required to reanalyze the data reported in this paper is available from the lead contact upon request

EXPERIMENTAL MODEL AND SUBJECT DETAILS

Human High-Altitude Studies—The human volunteer samples were obtained as part of the AltitudeOmics project(Ryan et al., 2014; Subudhi et al., 2014). In brief, all procedures conformed to the Declaration of Helsinki and were approved by the Institutional Review Boards at the University of Colorado and University of Oregon and the US Department of Defense Human Research Protection Office. The detailed experimental protocols were described previously(Ryan et al., 2014; Subudhi et al., 2014). Each participant in this study was healthy, a non-smoker, cardiorespiratory disease free, was born and raised at <1500 m, and had not traveled to elevations >1000 m in the 3 months before the investigation. The clinical characteristics of all participants in this study are described in Table S1 (Total n=18, male=11, female=7).

Animals—All animal protocols were in accordance with National Institutes of Health guidelines and approved by the Institutional Animal Welfare Committee of the University of Texas Health Science Center at Houston (AWC-19–0112). All experimental animals were housed under controlled conditions with temperature of 71F and humidity around 50%. The lights are programmed to start “sunrise” at 7am and “sunset” at 7pm. It takes +/− 15 minutes to complete the dimming or rising light process on either end, but it keeps the 12:12 light-dark cycle. Food and water were available ad libitum for all animals. *Tgm2*$^{flox/flox}$ mice were obtained from Gail VW Johnson (University of Rochester, New York) with permission from SE Iismaa and RM Graham (Victor Chang Cardiac Research Institute, Australia) (*Journal of Biological Chemistry* 2001;276, 20673–78). C57BL/6 mice (Stock No:000664) were purchased from Jackson Laboratory. Mice with an erythrocyte-specific deletion of *Tgm2* (*Tgm2*$^{flox/flox}$ *EpoR-Cre*$^{+}$) were generated by crossing *Tgm2*$^{flox/flox}$ mice with *EpoR-Cre*$^{+}$ mice(Heinrich et al., 2004). These mice were genotyped using specifically designed primers (*Tgm2*$^{flox/flox}$: GGCAAGGTCTGAGAAAGCAC, CACGTAGACTGTTCCCAGCA; *EpoRCre*$^{+}$: GTGTGGCTGCCCCTTCTGCCA, CAGGAATTCAAGCTCAACCTCA) and the expression of TG2 protein was determined by western blot (Figure S1b-S1c). Eight to 12 weeks, age matched male *EpoR-Cre*$^{+}$ mice and *Tgm2*$^{flox/flox}$ *EpoR-Cre*$^{+}$ mutant mice were used for experiments. Mice were anesthetized with isoflurane (2%), and each mouse was infused with AngII (500 ng/kg/min) or saline subcutaneously by implantation of an osmotic mini-pump (ALZET) through a small incision made in the nape of the mouse neck. For the rescue experiments, mice were randomly assigned to three groups. (i) control group: infused with saline via mini-pump and received saline i.p.; (ii) Ang II group: infused with Ang II (500ng/kg/min) via mini-pump and received saline i.p.; (iii) Ang II+L-carnitine group: infused with AngII (500ng/kg/min) via mini-pump and received L-carnitine (500mg/kg body weight/day, i.p.). For *in vivo* tracer experiment, mice were intravenously injected with 5% D-Glucose-1,2,3-^{13}C3 (5ml/kg) (Sigma) for 30min and then samples were collected. For all animal experiments, kidney, heart and liver were collected and either frozen immediately in liquid nitrogen or fixed in 10% buffered formalin phosphate (Fisher Scientific) for histochemical examination. For long-term storage, samples were stored in a −80°C freezer.

***In vitro* human and murine erythrocytes culture—**Both human and mouse blood were collected with heparin as an anti-coagulant and centrifuged at 2,000 x g for 5 min at room temperature, followed by percoll purification. Purified mature erythrocytes were washed three times with culture media (F-10 nutrient mix, Life Technology) and re-suspended to 4% hematocrit. The suspended RBCs were added to each well of a 12-well plate and treated with different concentrations of cystamine (Sigma, #30050) for 6 hour or for different time points.

Primary murine kidney organ culture—Kidneys were surgically isolated from C57BL/6 mice, washed 3 times in cold PBS, then dissected into 2–3 mm^3 pieces using autoclaved sterilized scissors and tweezers. Minced kidney explants were suspended in Dulbecco's modified Eagle Medium (DMEM, Gibco) with 10% fetal bovine serum (FBS, Corning) and cultured in a humidified atmosphere of 5% CO_2 at 37°C(Luo et al., 2015). After 24 hours, culture media was changed to DMEM without 10% FBS and treated with DMOG (Selleckchem, #S7483), Chrysin (Selleckchem, #S2281), Fenofibrate (Selleckchem, #S1794), L-carnitine (Selleckchem, #S2388) in normoxia (21% O_2,) or hypoxia condition (1% O_2,). Hypoxic challenge was performed using hypoxia chamber (Whitley H45 Hypoxystation). After treatment, total RNA and protein were isolated for quantitative RT-PCR and western blot analysis.

METHOD DETAILS

***In vivo* hypoxia challenge—**Hypoxic challenge was performed using hypoxia chamber (BioSpherix) with continued monitoring of oxygen concentration (BioSpherix, ProIx-110). In this study, oxygen concentration for the hypoxia challenge was 10%.

Mouse blood pressure measurement—Systolic blood pressure was measured using a carotid catheter-calibrated tail-cuff system (CODA, Kent Scientific, Torrington, CT), as previously described(Luo et al., 2015; Zhang et al.,2013). Briefly, mice were placed in temperature-controlled chambers (37°C) and blood pressure was monitored before mini-pump implantation, which was considered as baseline and continuously measured after mini-pump surgery. For every episode of blood pressure measurement, the first five cycles of blood pressure measurement were deemed as an initial acclimatization, followed by a period of 20 cycles of blood pressure measurement. The averaged value of the 20 cycles was used for the analysis of blood pressure.

24 hour-urine collection and analysis—Mice were placed in metabolic cages (Nalgene) for 24 hour-urine collection. The urine albumin and creatinine were measured by commercially available kits (Exocell 1011 and 1012) without any modification as previously described(Peng et al., 2019).

Erythrocytes and plasma collection—Mouse blood was collected in EDTA anticoagulated tubes (MiniCollect), then centrifuged at 3000 rpm for 5 min at 4°C. Plasma was collected in the upper layer, and packed cells were collected at the bottom. Mature red blood cells were purified via 70% Percoll density centrifugation (Sigma).

Quantification of erythrocyte 2,3-BPG level and P50—Twenty μl of whole blood was added into 100 μl, 0.6 M cold perchloric acid on ice and mixed well, followed by centrifugation at 13,000rpm for 10 min. Eighty μl of supernatant was transferred to a new tube, then neutralized with 10 μl 2.5 M K_2CO_3, followed by centrifugation at 13,000rpm for 10 min. A volume of 10 μl supernatant was used to quantify 2,3-BPG using a commercially available kit (Roche)(Sun et al., 2016). For P50(Liu et al., 2016), 10 μl of whole blood aliquot was added into 3 ml Hemox Buffer (TCS Scientific Corporation) with 5 μl anti-foaming reagent (TCS Scientific Corporation) and 5 μl 22% BSA in PBS. The mixture was then added into Hemox Analyzer (TCS Scientific Corporation) to measure the oxygen equilibrium curve at 37 °C.

BPGM activity measurement—Erythrocytes were lysed in cold ddH_2O with protease inhibitors. Twenty-five μg of erythrocyte protein lysates were utilized for measurement of 2,3-BPG mutase activity as described previously(Liu et al., 2016). Briefly, erythrocyte protein extract was incubated in 100 μl prepared reaction mixture (100 mM Triethanolamine pH 7.6, 1 mM MgSO4, 4 mM ATP, 3 mM 3-phosphoglycerate, 10 units phosphoglycerate kinase) for 30 minutes at room temperature. The reaction was stopped by adding 5 μl of 11.63 M perchloric acid. The reaction system was incubated on ice for 10 min, then spun at 14,000rpm for 5 min at 4°C. Eighty μl supernatant was transferred to a new tube, then neutralized with 10 μl 2.5 M K_2CO_3, vortexed and incubated on ice for 10 min. Subsequently the reaction was centrifuged at 14,000rpm for 10 minutes, 10 μl supernatant was collected for 2,3-BPG measurement by using a commercial assay (Roche), as previously described(Peng et al., 2019).

TG2 activity assay—TG2 activity in RBC samples was determined with Transglutaminase Assay Kit (Sigma-Aldrich, #CS1070) following manufacturer's instructions except using 37°C as the reaction incubation temperature, as previously described(Liu et al., 2015; Luo et al., 2016).

ATP level measurement—ATP levels were determined with ATP Colorimetric/ Fluorometric Assay Kit (BioVision, # K354–100) following manufacturer's instructions.

Erythrocyte membrane isolation—Purified mature red blood cells were washed three times with cold PBS (Gibco). The RBC pellet (100 ul) was lysed with 5 ml 0.4% NaCl with 1X protease (ThermoFisher) and phosphatase inhibitors (Roche), and incubated on ice for 15 min with occasional vortexing. The lysate was spun at 3000rpm for 10 min at 4 °C. The supernatant was discarded, 5 ml 0.4% NaCl with 1X protease and phosphatase inhibitors was added, then the lysate was vortexed and centrifuged 3000rpm for 10 min at 4 °C. The previous centrifuging step was repeated for a total of 5 times. The pellet was suspended in 100 ul RIPA buffer, sonicated for 10 seconds twice. The lysate was incubated on ice for 30 min, then centrifuged at 15,000 x g for 10 min at 4 °C. The supernatant was saved and stored at −80 °C for future use.

Immunoprecipitation—Immunoprecipitation (IP) was performed in 0.5 ml IP solution (protein lysate and IP buffer (50 mM Tris-HCl pH 7.5, 150 mM NaCl and 1% triton x-100) along with protease inhibitor and 20 mM N-ethylmaleimide). Ubiquitin (Santa Cruz,

#sc-8017, 1:100) and BPGM (Proteintech, #17173–1-AP, 1:1,00) antibodies were added to the IP solution respectively, followed by incubation overnight at 4 °C. After primary antibody incubation, 50 ul Protein G Sepharose beads (GE Healthcare Life Sciences, #:17–0618-01) was added and incubated at 4 °C overnight or at room temperature for 2 h. Beads conjugated with anti-ε-(γ-glutamyl)-lysine isopeptide IgM (81D4) (Covalab, #opr0003) was used to pull down proteins with isopeptide bonds. IP proteins were eluted by boiling in 30 ml 2 X Laemmli Sample Buffer (Bio-Rad, #:1610737) at 100 °C for 10 min and resolved on 10% SDS–PAGE gels for western blot.

Western blot analysis—Erythrocytes were lysed in H2O at 1:10 volume ratio in the presence of 1X protease inhibitor cocktail (Roche, #11697498001), 1X phosphatase inhibitor cocktail (Roche, #04906837001) and proteasome inhibitor MG132 (Santa Cruz, #sc-201270) 10uM or Bortezomib (Santa Cruz, #sc-217785) 1uM, then 10X PBS was added to the lysate to neutralize buffer. Protein concentration was determined by BCA Protein Assay kit (Pierce). Protein samples were boiled in Laemmli Sample Buffer (Bio-Rad) for 10 min at 95 °C, then loaded to 10% SDS–PAGE gel for western blot. We used antibodies to OCTN2 (Abcam, #ab180757, 1:1,000), TG2 (GeneTex, #GTX111702, 1:1,000), BPGM (Proteintech, #17173–1-AP, 1:1,000), GAPDH (Invitrogen, # PA1–987, 1:1,000), Isopeptide [81D1C2] (Abcam, #ab422, 1:1,000), Ubiquitin (Santa Cruz, #sc-8017, 1:1000), PPARα (Invitrogen, #PA585125, 1:1000), HIF-1α (Invitrogen, #PA1–16601,1:1000) and β-Actin (Cell Signaling, #3700S,1:2000). The secondary antibodies were obtained from LI-COR (IRDye 800CW Donkey anti-Rabbit IgG, #926–32213, 1:10000; IRDye 680RD Donkey anti-Mouse IgG, #926–68072, 1:10000) and all secondary antibodies were used at 100 ng ml^{-1} in LI-COR blocking buffer （LI-COR, #927–40000） supplied with 0.2% Tween 20.

Western blots were scanned by Odyssey Imaging System (LI-COR) following the manufacturer's instructions. Protein bands were quantified by densitometry, expressed relative to β-actin and normalized as indicated in the figure legends for each condition.

Reverse transcription polymerase chain reaction (RT-PCR)—Total RNA was isolated from tissue using TRIzol (Life Technologies) following the manufacturer's instructions. Complementary DNA (cDNA) was generated using the reverse transcription kit (QIAGEN). Relative gene expression was quantified using a SYBR Green PCR kit (QIAGEN). The primers for quantification were purchased from IDT (Integrated DNA Technologies, Inc.). The sequences of primers shown in Table S2.

Metabolomics analysis—Analyses were performed as previously described(D'Alessandro et al., 2019; Nemkov et al., 2020). Briefly, RBC, plasma, urine and kidney extracts were extracted in methanol: acetonitrile: water 5:3:2 (v/v/v) as described(D'Alessandro et al., 2019; Nemkov et al., 2020). After incubation at 4 °C for 30 min with constant agitation, the supernatants were separated by centrifugation (10,000 x g for 10 min at 4 °C) and stored at −80 °C until analysis. Samples were vortexed(Reisz et al., 2018) and insoluble material pelleted as described(D'Alessandro et al., 2017; Nemkov et al., 2016). Ultra-High-Pressure Liquid Chromatography-Mass Spectrometry metabolomics analyses were performed using a Vanquish UHPLC coupled online to a Q Exactive mass spectrometer (Thermo Fisher, Bremen, Germany). Samples were analyzed using a

3 minute(Nemkov et al., 2017) isocratic condition or a 5 min gradient as described (Nemkov et al., 2019). Solvents were supplemented with 0.1% formic acid for positive mode runs and 1 mM ammonium acetate for negative mode runs. MS acquisition, data analysis and elaboration were performed as described(Nemkov et al., 2019). Additional analyses, including untargeted analyses and Fish score calculation via MS/MS, were calculated against the ChemSpider database with Compound Discoverer 2.0 (Thermo Fisher, Bremen, Germany). Metabolic pathway analysis and statistical analyses were performed using the MetaboAnalyst 4.0(Chong et al., 2018).

Mass spectrometric analysis—The samples were loaded onto a 1.5 mm thick NuPAGE Bis-Tris 4−12% gradient gel (Invitrogen) and visualized with SimplyBlue™ SafeStain (Invitrogen) stain. Each lane of the gel was divided into 4 equal-sized bands, and proteins in the gel were digested as follows. The pieces were destained in 200 μl of 25 mM ammonium bicarbonate in 50% (v/v) acetonitrile for 15 min and washed with 200 μl of 50% (v/v) acetonitrile. Disulfide bonds were reduced by dithiothreitol, and cysteine residues were alkylated with iodoacetamide. Modified sequencing grade trypsin (Promega) was added 1:100 (w/w) and the samples were digested overnight at 37 C. The digestion was stopped by addition of 5% formic acid (FA). Organic solvent was removed in a SpeedVac concentrator and resuspended in 40 ul of 0.1% FA. Each sample was loaded onto individual Evotips for desalting and then washed with 200 μl 0.1% FA followed by the addition of 100 μl storage solvent (0.1% FA) to keep the Evotips wet until analysis. The Evosep One system (Evosep, Odense, Denmark) was used to separate peptides on a Pepsep column, (150 um inner diameter, 15 cm) packed with ReproSil C18 1.9 um, 120A resin. The system was coupled to the timsTOF Pro mass spectrometer (Bruker Daltonics, Bremen, Germany) via the nano-electrospray ion source (Captive Spray, Bruker Daltonics). The mass spectrometer was operated in PASEF mode. The ramp time was set to 100 ms and 10 PASEF MS/MS scans per topN acquisition cycle were acquired. MS and MS/MS spectra were recorded from *m/z* 100 to 1700. The ion mobility was scanned from 0.7 to 1.50 Vs/cm^2. Precursors for data-dependent acquisition were isolated within ± 1 Th and fragmented with an ion mobility-dependent collision energy, which was linearly increased from 20 to 59 eV in positive mode. Low-abundance precursor ions with an intensity above a threshold of 500 counts but below a target value of 20000 counts were repeatedly scheduled and otherwise dynamically excluded for 0.4 min.

Database Searching and Protein Identification—MS/MS spectra were extracted from raw data files and converted into .mgf files using MS Convert (ProteoWizard, Ver. 3.0). Peptide spectral matching was performed with Mascot (Ver. 2.5) against the Uniprot mouse database. Mass tolerances were +/− 15 ppm for parent ions, and +/− 0.4 Da for fragment ions. Trypsin specificity was used, allowing for 1 missed cleavage. Met oxidation, protein N-terminal acetylation, isopeptide bond formation with loss of ammonia (K) and peptide N-terminal pyroglutamic acid formation were set as variable modifications with Cys carbamidomethylation set as a fixed modification.

Scaffold (version 4.8, Proteome Software, Portland, OR, USA) was used to validate MS/MS based peptide and protein identifications. Peptide identifications were accepted if they

could be established at greater than 95.0% probability as specified by the Peptide Prophet algorithm. Protein identifications were accepted if they could be established at greater than 99.0% probability and contained at least two identified unique peptides.

Gene Ontology biological processes analysis—To interpret the specific pathways associated with TG2 mediated isopeptide modification, genes in selected modules were analyzed using the online bioinformatics database Metascape as previously described(Zhou et al., 2019) (http://metascape.org/gp/index.html#/main/step1). For given gene list, process enrichment analysis has been carried out with GO Biological Processes. Bar graph demonstrating biological processes enrichment analysis of up-regulated proteins from isopeptide pulldown comparing *EpoR-Cre*$^{+}$ and *Tgm2*$^{f/f}$ *EpoR-Cre*$^{+}$ RBCs.

Plasma creatinine and urea measurement—Plasma creatinine levels were determined with a creatinine colorimetric assay kit (Abcam, #ab65340) following the manufacturer's instructions. Plasma urea concentrations were determined by using a urea assay kit (Sigma-Aldrich, #MAK006), which utilizes a coupled enzyme reaction, resulting in a colorimetric (570 nm) product.

RBC ROS detection by flow cytometry—RBC ROS level was evaluated by flow cytometry according to the manufacturer's recommended protocol. Briefly, 1 ul RBC pellet was resuspended in 100 ul PBS and incubated with CM-H2DCFDA (Invitrogen, C6827) at 1.73 uM for 30 minutes at 37 °C in the dark. Samples were then washed 3 times with PBS and resuspended with 200 ul PBS. Samples were analyzed for fluorescence in the fluorescein isothiocyanate (FITC) channel on a BD FACS-Canto cytometer using BD FacsDiva software (version 6.2).

Histological analysis—Mouse hearts, livers and kidneys were fixed in 10% buffered formalin phosphate, then were sent to the Histology Laboratory (Department of Pathology and Laboratory Medicine, McGovern Medical School, University of Texas) for sectioning (5 μm) and hematoxylin and eosin stain (H&E) or Masson's trichrome staining. Slides were examined by light microscopy and assessed for kidney morphology and fibrosis. Renal injury score of H&E staining was assessed by quantifying the chronic kidney disease features in glomeruli and tubules, as previous described(Zhang et al., 2013). The score was counted in 10 fields of randomized and blinded slides with each field having at least 15 glomeruli and tubules, respectively. A highest score of 5 was accorded to complete loss of capillary space and sclerosis or necrosis. A score of 1 was assigned to normal amount of capillary space within Bowman's capsule and normal structures of tubules. An intermediate score of 3 was assigned to the damage between complete loss of capillary space and normal capilary space. Renal fibrosis score, defined as the percentage of the blue area (section with positive staining for collagen) relative to the whole area of the field, was calculated using ImageJ computer software.

Hypoxyprobe immunofluorescence measurement—Tissue hypoxia levels were measured by Hypoxyprobe immunofluorescence intensity as described before(Sun et al., 2016). Briefly, mice were injected with 50 mg/kg Hypoxyprobe (Hypoxyprobe, Inc.) 30 min before tissues were harvested. Tissues were fixed in 10% buffered formalin and sent

to the Histology Laboratory for sectioning (5 μm). Sides were rehydrated, permeabilized with 0.5% Triton X-100 in PBS for 20 min, blocked in 3% BSA in PBS and incubated in anti-hypoxyprobe antibody (Hypoxyprobe, Inc., rabbit anti-PAb2627AP) overnight at 4 °C. Alexa Fluor 594-conjugated donkey anti-rabbit IgG antibody (Life Technologies) was used as a secondary antibody for Hypoxyprobe immunofluorescence. After washing, slides were sealed with ProLong Gold Antifade Reagent (Invitrogen). Quantification of the fluorescent intensity was performed using the Image-J software. The average immunofluorescence density of 5 fields per slide was used for analysis.

QUANTIFICATION AND STATISTICAL ANALYSIS

Statistical Analysis—All data are expressed as mean ± SD. Statistical analyses were performed with Graphpad Prism (version 8.3.1). Statistical significance was determined using Unpaired t-test based on sample distribution for comparing differences between 2 groups. One-way ANOVA was applied to analyze mean differences among multiple groups, followed by a Tukey multiple-comparisons test. Two-way ANOVA was used to compare data collected from different time points and dosages, followed by Tukey or Sidak post hoc test. A value of $P<0.05$ was considered to denote statistical significance.

Supplementary Material

Refer to Web version on PubMed Central for supplementary material.

Acknowledgments

This work was supported by HL136969 (YX), HL137990 (YX), McGovern Fund (YX) and the Bob and Hazel Casey Endowed Chair (REK) of University of Texas Health Science Center-McGovern Medical School; R01HL146442, R01HL149714, R01HL148151, R21HL150032 (AD); W81XWH-11-2-0040 TATRC (RR).

References

Akimov SS, Krylov D, Fleischman LF, and Belkin AM (2000). Tissue transglutaminase is an integrin-binding adhesion coreceptor for fibronectin. J Cell Biol 148, 825–838. [PubMed: 10684262]

Arce SC (2017). Long-Term Oxygen for COPD. N Engl J Med 376, 286–287.

Bärtsch P, and Gibbs JS (2007). Effect of altitude on the heart and the lungs. Circulation 116, 2191–2202. [PubMed: 17984389]

Basnyat B. (2013). Acute high-altitude illnesses. N Engl J Med 369, 1666.

Benesch R, and Benesch RE (1969). Intracellular organic phosphates as regulators of oxygen release by haemoglobin. Nature 221, 618–622. [PubMed: 5774935]

Berg AH, Drechsler C, Wenger J, Buccafusca R, Hod T, Kalim S, Ramma W, Parikh SM, Steen H, Friedman DJ, et al. (2013). Carbamylation of serum albumin as a risk factor for mortality in patients with kidney failure. Science translational medicine 5, 175ra129.

Bergamini CM (1988). GTP modulates calcium binding and cation-induced conformational changes in erythrocyte transglutaminase. FEBS Lett 239, 255–258. [PubMed: 2903073]

Bernauer C, Man YKS, Chisholm JC, Lepicard EY, Robinson SP, and Shipley JM (2021). Hypoxia and its therapeutic possibilities in paediatric cancers. Br J Cancer 124, 539–551. [PubMed: 33106581]

Biernatowska A, Augoff K, Podkalicka J, Tabaczar S, Gajdzik-Nowak W, Czogalla A, and Sikorski AF (2017). MPP1 directly interacts with flotillins in erythrocyte membrane - Possible mechanism of raft domain formation. Biochimica et biophysica acta. Biomembranes 1859, 2203–2212. [PubMed: 28865798]

Bissinger R, Nemkov T, A DA, Grau M, Dietz T, Bohnert BN, Essigke D, Worn M, Schaefer L, Xiao M, et al. (2021). Proteinuric chronic kidney disease is associated with altered red blood cell lifespan, deformability and metabolism. Kidney Int.

Chang TT, Shyu MK, Huang MC, Hsu CC, Yeh SY, Chen MR, and Lin CJ (2011). Hypoxia-mediated down-regulation of OCTN2 and PPARα expression in human placentas and in BeWo cells. Molecular pharmaceutics 8, 117–125. [PubMed: 21125992]

Chong J, Soufan O, Li C, Caraus I, Li S, Bourque G, Wishart DS, and Xia J. (2018). MetaboAnalyst 4.0: towards more transparent and integrative metabolomics analysis. Nucleic Acids Res 46, W486–w494. [PubMed: 29762782]

D'Alessandro A, Culp-Hill R, Reisz JA, Anderson M, Fu X, Nemkov T, Gehrke S, Zheng C, Kanias T, Guo Y, et al. (2019). Heterogeneity of blood processing and storage additives in different centers impacts stored red blood cell metabolism as much as storage time: lessons from REDS-III-Omics. Transfusion 59, 89–100. [PubMed: 30353560]

D'Alessandro A, Nemkov T, Yoshida T, Bordbar A, Palsson BO, and Hansen KC (2017). Citrate metabolism in red blood cells stored in additive solution-3. Transfusion 57, 325–336. [PubMed: 27813142]

D'Alessandro A, and Xia Y. (2020). Erythrocyte adaptive metabolic reprogramming under physiological and pathological hypoxia. Curr Opin Hematol 27, 155–162. [PubMed: 32141895]

D'Alessandro A, Moore HB, Moore EE, Reisz JA, Wither MJ, Ghasasbyan A, Chandler J, Silliman CC, Hansen KC, and Banerjee A. (2017). Plasma succinate is a predictor of mortality in critically injured patients. J Trauma Acute Care Surg 83, 491–495. [PubMed: 28590356]

Di Liberato L, Arduini A, Rossi C, Di Castelnuovo A, Posari C, Sacchetta P, Urbani A, and Bonomini M. (2014). L-Carnitine status in end-stage renal disease patients on automated peritoneal dialysis. J Nephrol 27, 699–706. [PubMed: 24599831]

Eckert RL, Kaartinen MT, Nurminskaya M, Belkin AM, Colak G, Johnson GV, and Mehta K. (2014). Transglutaminase regulation of cell function. Physiol Rev 94, 383–417. [PubMed: 24692352]

El-Hattab AW, and Scaglia F. (2015). Disorders of carnitine biosynthesis and transport. Mol Genet Metab 116, 107–112. [PubMed: 26385306]

Ellsworth ML, Ellis CG, Goldman D, Stephenson AH, Dietrich HH, and Sprague RS (2009). Erythrocytes: oxygen sensors and modulators of vascular tone. Physiology (Bethesda) 24, 107–116. [PubMed: 19364913]

Fesus L, and Piacentini M. (2002). Transglutaminase 2: an enigmatic enzyme with diverse functions. Trends Biochem Sci 27, 534–539. [PubMed: 12368090]

Forrester SJ, Booz GW, Sigmund CD, Coffman TM, Kawai T, Rizzo V, Scalia R, and Eguchi S. (2018). Angiotensin II Signal Transduction: An Update on Mechanisms of Physiology and Pathophysiology. Physiol Rev 98, 1627–1738. [PubMed: 29873596]

Fu Q, Colgan SP, and Shelley CS (2016). Hypoxia: The Force that Drives Chronic Kidney Disease. Clin Med Res 14, 15–39. [PubMed: 26847481]

Guder WG, and Wagner S. (1990). The role of the kidney in carnitine metabolism. J Clin Chem Clin Biochem 28, 347–350. [PubMed: 2199595]

Hackett PH, and Roach RC (2001). High-altitude illness. N Engl J Med 345, 107–114. [PubMed: 11450659]

Hammarlund EU, Flashman E, Mohlin S, and Licausi F. (2020). Oxygen-sensing mechanisms across eukaryotic kingdoms and their roles in complex multicellularity. Science 370.

Hasegawa G, Suwa M, Ichikawa Y, Ohtsuka T, Kumagai S, Kikuchi M, Sato Y, and Saito Y. (2003). A novel function of tissue-type transglutaminase: protein disulphide isomerase. Biochem J 373, 793–803. [PubMed: 12737632]

Heinrich AC, Pelanda R, and Klingmuller U. (2004). A mouse model for visualization and conditional mutations in the erythroid lineage. Blood 104, 659–666. [PubMed: 15090451]

Hershko A, Ciechanover A, and Varshavsky A. (2000). Basic Medical Research Award. The ubiquitin system. Nat Med 6, 1073–1081. [PubMed: 11017125]

Hsu YJ, Lin CW, Cho SL, Yang WS, Yang CM, and Yang CH (2020). Protective Effect of Fenofibrate on Oxidative Stress-Induced Apoptosis in Retinal-Choroidal Vascular Endothelial Cells: Implication for Diabetic Retinopathy Treatment. Antioxidants (Basel) 9.

Ientile R, Caccamo D, and Griffin M. (2007). Tissue transglutaminase and the stress response. Amino Acids 33, 385–394. [PubMed: 17390097]

Iismaa SE, Mearns BM, Lorand L, and Graham RM (2009). Transglutaminases and disease: lessons from genetically engineered mouse models and inherited disorders. Physiol Rev 89, 991–1023. [PubMed: 19584319]

Iyer NV, Kotch LE, Agani F, Leung SW, Laughner E, Wenger RH, Gassmann M, Gearhart JD, Lawler AM, Yu AY, et al. (1998). Cellular and developmental control of O2 homeostasis by hypoxia-inducible factor 1 alpha. Genes Dev 12, 149–162. [PubMed: 9436976]

Jang GY, Jeon JH, Cho SY, Shin DM, Kim CW, Jeong EM, Bae HC, Kim TW, Lee SH, Choi Y, et al. (2010). Transglutaminase 2 suppresses apoptosis by modulating caspase 3 and NF-kappaB activity in hypoxic tumor cells. Oncogene 29, 356–367. [PubMed: 19838207]

Kakhniashvili DG, Bulla LA Jr., and Goodman SR (2004). The human erythrocyte proteome: analysis by ion trap mass spectrometry. Mol Cell Proteomics 3, 501–509. [PubMed: 14963112]

Kang HM, Ahn SH, Choi P, Ko YA, Han SH, Chinga F, Park AS, Tao J, Sharma K, Pullman J, et al. (2015). Defective fatty acid oxidation in renal tubular epithelial cells has a key role in kidney fibrosis development. Nat Med 21, 37–46. [PubMed: 25419705]

Komander D, and Rape M. (2012). The ubiquitin code. Annu Rev Biochem 81, 203–229. [PubMed: 22524316]

Lee P, Chandel NS, and Simon MC (2020). Cellular adaptation to hypoxia through hypoxia inducible factors and beyond. Nat Rev Mol Cell Biol 21, 268–283. [PubMed: 32144406]

Lenfant C, Torrance J, English E, Finch CA, Reynafarje C, Ramos J, and Faura J. (1968). Effect of altitude on oxygen binding by hemoglobin and on organic phosphate levels. The Journal of clinical investigation 47, 2652–2656. [PubMed: 5725278]

Lewis IA, Campanella ME, Markley JL, and Low PS (2009). Role of band 3 in regulating metabolic flux of red blood cells. Proc Natl Acad Sci U S A 106, 18515–18520. [PubMed: 19846781]

Liu C, Luo R, Elliott SE, Wang W, Parchim NF, Iriyama T, Daugherty PS, Blackwell SC, Sibai BM, Kellems RE, et al. (2015). Elevated Transglutaminase Activity Triggers Angiotensin Receptor Activating Autoantibody Production and Pathophysiology of Preeclampsia. J Am Heart Assoc 4.

Liu H, Zhang Y, Wu H, D'Alessandro A, Yegutkin GG, Song A, Sun K, Li J, Cheng NY, Huang A, et al. . (2016). Beneficial Role of Erythrocyte Adenosine A2B Receptor-Mediated AMP-Activated Protein Kinase Activation in High-Altitude Hypoxia. Circulation 134, 405–421. [PubMed: 27482003]

Low PS, Rathinavelu P, and Harrison ML (1993). Regulation of glycolysis via reversible enzyme binding to the membrane protein, band 3. The Journal of biological chemistry 268, 14627–14631. [PubMed: 8325839]

Luks AM, Johnson RJ, and Swenson ER (2008). Chronic kidney disease at high altitude. J Am Soc Nephrol 19, 2262–2271. [PubMed: 18842990]

Luo H, Zhang Y, Guo H, Zhang L, Li X, Ringseis R, Wen G, Hui D, Liang A, Eder K, et al. (2014). Transcriptional regulation of the human, porcine and bovine OCTN2 gene by PPARα via a conserved PPRE located in intron 1. BMC genetics 15, 90. [PubMed: 25299939]

Luo R, Liu C, Elliott SE, Wang W, Parchim N, Iriyama T, Daugherty PS, Tao L, Eltzschig HK, Blackwell SC, et al. (2016). Transglutaminase is a Critical Link Between Inflammation and Hypertension. J Am Heart Assoc 5.

Luo R, Zhang W, Zhao C, Zhang Y, Wu H, Jin J, Zhang W, Grenz A, Eltzschig HK, Tao L, et al. (2015). Elevated Endothelial Hypoxia-Inducible Factor-1alpha Contributes to Glomerular Injury and Promotes Hypertensive Chronic Kidney Disease. Hypertension 66, 75–84. [PubMed: 25987665]

Maeda T, Wakasawa T, Funabashi M, Fukushi A, Fujita M, Motojima K, and Tamai I. (2008). Regulation of Octn2 transporter (SLC22A5) by peroxisome proliferator activated receptor alpha. Biological & pharmaceutical bulletin 31, 1230–1236. [PubMed: 18520060]

McGettrick AF, and O'Neill LAJ (2020). The Role of HIF in Immunity and Inflammation. Cell metabolism 32, 524–536. [PubMed: 32853548]

Mi Z, Si T, Kapadia K, Li Q, and Muma NA (2017). Receptor-stimulated transamidation induces activation of Rac1 and Cdc42 and the regulation of dendritic spines. Neuropharmacology 117, 93–105. [PubMed: 28161375]

Mishra S, Saleh A, Espino PS, Davie JR, and Murphy LJ (2006). Phosphorylation of histones by tissue transglutaminase. J Biol Chem 281, 5532–5538. [PubMed: 16407273]

Nakaoka H, Perez DM, Baek KJ, Das T, Husain A, Misono K, Im MJ, and Graham RM (1994). Gh: a GTP-binding protein with transglutaminase activity and receptor signaling function. Science 264, 1593–1596. [PubMed: 7911253]

Narravula S, and Colgan SP (2001). Hypoxia-inducible factor 1-mediated inhibition of peroxisome proliferator-activated receptor alpha expression during hypoxia. Journal of immunology (Baltimore, Md. : 1950) 166, 7543–7548.

Nemkov T, Hansen KC, and D'Alessandro A. (2017). A three-minute method for highthroughput quantitative metabolomics and quantitative tracing experiments of central carbon and nitrogen pathways. Rapid Commun Mass Spectrom 31, 663–673. [PubMed: 28195377]

Nemkov T, Hansen KC, Dumont LJ, and D'Alessandro A. (2016). Metabolomics in transfusion medicine. Transfusion 56, 980–993. [PubMed: 26662506]

Nemkov T, Qadri SM, Sheffield WP, and D'Alessandro A. (2020). Decoding the metabolic landscape of pathophysiological stress-induced cell death in anucleate red blood cells. Blood Transfus, 1–16.

Nemkov T, Reisz JA, Gehrke S, Hansen KC, and D'Alessandro A. (2019). High-Throughput Metabolomics: Isocratic and Gradient Mass Spectrometry-Based Methods. Methods Mol Biol 1978, 13–26. [PubMed: 31119654]

Peng Z, Luo R, Xie T, Zhang W, Liu H, Wang W, Tao L, Kellems RE, and Xia Y. (2019). Erythrocyte Adenosine A2B Receptor-Mediated AMPK Activation: A Missing Component Counteracting CKD by Promoting Oxygen Delivery. J Am Soc Nephrol 30, 1413–1424. [PubMed: 31278195]

Rahman SM, Qadri I, Janssen RC, and Friedman JE (2009). Fenofibrate and PBA prevent fatty acid-induced loss of adiponectin receptor and pAMPK in human hepatoma cells and in hepatitis C virus-induced steatosis. J Lipid Res 50, 2193–2202. [PubMed: 19502591]

Reisz JA, Nemkov T, Dzieciatkowska M, Culp-Hill R, Stefanoni D, Hill RC, Yoshida T, Dunham A, Kanias T, Dumont LJ, et al. (2018). Methylation of protein aspartates and deamidated asparagines as a function of blood bank storage and oxidative stress in human red blood cells. Transfusion 58, 2978–2991. [PubMed: 30312994]

Robledo RF, Lambert AJ, Birkenmeier CS, Cirlan MV, Cirlan AF, Campagna DR, Lux SE, and Peters LL (2010). Analysis of novel sph (spherocytosis) alleles in mice reveals allele-specific loss of band 3 and adducin in alpha-spectrin-deficient red cells. Blood 115, 1804–1814. [PubMed: 20056793]

Rogers SC, Ross JG, d'Avignon A, Gibbons LB, Gazit V, Hassan MN, McLaughlin D, Griffin S, Neumayr T, Debaun M, et al. (2013). Sickle hemoglobin disturbs normal coupling among erythrocyte O2 content, glycolysis, and antioxidant capacity. Blood 121, 1651–1662. [PubMed: 23297128]

Rogers SC, Said A, Corcuera D, McLaughlin D, Kell P, and Doctor A. (2009). Hypoxia limits antioxidant capacity in red blood cells by altering glycolytic pathway dominance. FASEB J 23, 3159–3170. [PubMed: 19417084]

Ryan BJ, Wachsmuth NB, Schmidt WF, Byrnes WC, Julian CG, Lovering AT, Subudhi AW, and Roach RC (2014). AltitudeOmics: rapid hemoglobin mass alterations with early acclimatization to and de-acclimatization from 5260 m in healthy humans. PLoS One 9, e108788.

Semenza GL (2014). Hypoxia-inducible factor 1 and cardiovascular disease. Annu Rev Physiol 76, 39–56. [PubMed: 23988176]

Siegel M, and Khosla C. (2007). Transglutaminase 2 inhibitors and their therapeutic role in disease states. Pharmacol Ther 115, 232–245. [PubMed: 17582505]

Song A, Zhang Y, Han L, Yegutkin GG, Liu H, Sun K, D'Alessandro A, Li J, Karmouty-Quintana H, Iriyama T, et al. (2017). Erythrocytes retain hypoxic adenosine response for faster acclimatization upon re-ascent. Nat Commun 8, 14108. [PubMed: 28169986]

Su T, Qin XY, and Furutani Y. (2021). Transglutaminase 2 as a Marker for Inflammation and Therapeutic Target in Sepsis. Int J Mol Sci 22.

Subudhi AW, Bourdillon N, Bucher J, Davis C, Elliott JE, Eutermoster M, Evero O, Fan JL, Jameson-Van Houten S, Julian CG, et al. (2014). AltitudeOmics: the integrative physiology of human acclimatization to hypobaric hypoxia and its retention upon reascent. PLoS One 9, e92191.

Sun K, Zhang Y, D'Alessandro A, Nemkov T, Song A, Wu H, Liu H, Adebiyi M, Huang A, Wen YE, et al. (2016). Sphingosine-1-phosphate promotes erythrocyte glycolysis and oxygen release for adaptation to high-altitude hypoxia. Nat Commun 7, 12086. [PubMed: 27417539]

Voit RA, and Sankaran VG (2020). Stabilizing HIF to Ameliorate Anemia. Cell 180, 6. [PubMed: 31951520]

Vyas FS, Hargreaves AJ, Bonner PL, Boocock DJ, Coveney C, and Dickenson JM (2016). A1 adenosine receptor-induced phosphorylation and modulation of transglutaminase 2 activity in H9c2 cells: A role in cell survival. Biochemical pharmacology 107, 41–58. [PubMed: 27005940]

Wen G, Ringseis R, and Eder K. (2010). Mouse OCTN2 is directly regulated by peroxisome proliferator-activated receptor alpha (PPARalpha) via a PPRE located in the first intron. Biochemical pharmacology 79, 768–776. [PubMed: 19819229]

West JB (2004). The physiologic basis of high-altitude diseases. Ann Intern Med 141, 789–800. [PubMed: 15545679]

Wojtal KA, Cee A, Lang S, Götze O, Frühauf H, Geier A, Pastor-Anglada M, Torres-Torronteras J, Martí R, Fried M, et al. (2014). Downregulation of duodenal SLC transporters and activation of proinflammatory signaling constitute the early response to high altitude in humans. American journal of physiology. Gastrointestinal and liver physiology 307, G673–688. [PubMed: 24970780]

Wu H, Bogdanov M, Zhang Y, Sun K, Zhao S, Song A, Luo R, Parchim NF, Liu H, Huang A, et al. (2016). Hypoxia-mediated impaired erythrocyte Lands' Cycle is pathogenic for sickle cell disease. Sci Rep 6, 29637. [PubMed: 27436223]

Wu X, Huang W, Prasad PD, Seth P, Rajan DP, Leibach FH, Chen J, Conway SJ, and Ganapathy V. (1999). Functional characteristics and tissue distribution pattern of organic cation transporter 2 (OCTN2), an organic cation/carnitine transporter. J Pharmacol Exp Ther 290, 1482–1492. [PubMed: 10454528]

Xie T, Chen C, Peng Z, Brown BC, Reisz JA, Xu P, Zhou Z, Song A, Zhang Y, Bogdanov MV, et al. (2020a). Erythrocyte Metabolic Reprogramming by Sphingosine 1Phosphate in Chronic Kidney Disease and Therapies. Circ Res 127, 360–375. [PubMed: 32284030]

Xie T, Chen C, Peng Z, Brown BC, Reisz JA, Xu P, Zhou Z, Song A, Zhang Y, Bogdanov MV, et al. (2020b). Erythrocyte Metabolic Reprogramming by Sphingosine 1Phosphate in Chronic Kidney Disease and Therapies. Circulation research.

Zhang W, Zhang Y, Wang W, Dai Y, Ning C, Luo R, Sun K, Glover L, Grenz A, Sun H, et al. (2013). Elevated ecto-5'-nucleotidase-mediated increased renal adenosine signaling via A2B adenosine receptor contributes to chronic hypertension. Circulation research 112, 1466–1478. [PubMed: 23584256]

Zhou Y, Zhou B, Pache L, Chang M, Khodabakhshi AH, Tanaseichuk O, Benner C, and Chanda SK (2019). Metascape provides a biologist-oriented resource for the analysis of systems-level datasets. Nat Commun 10, 1523. [PubMed: 30944313]

Zonca S, Pinton G, Wang Z, Soluri MF, Tavian D, Griffin M, Sblattero D, and Moro L. (2017). Tissue transglutaminase (TG2) enables survival of human malignant pleural mesothelioma cells in hypoxia. Cell Death Dis 8, e2592. [PubMed: 28151477]

Highlights

- Hypoxia induces erythrocyte TG2 activity in healthy humans and mouse models.
- eTG2 mediated PTM of BPGM promotes its proteostasis, enhancing O_2 offload.
- eTG2 controls carnitine homeostasis by maintaining renal *Slc22a5* transcription in CKD.
- Carnitine supplementation ameliorates hypertension and CKD by enhancing oxygen delivery.

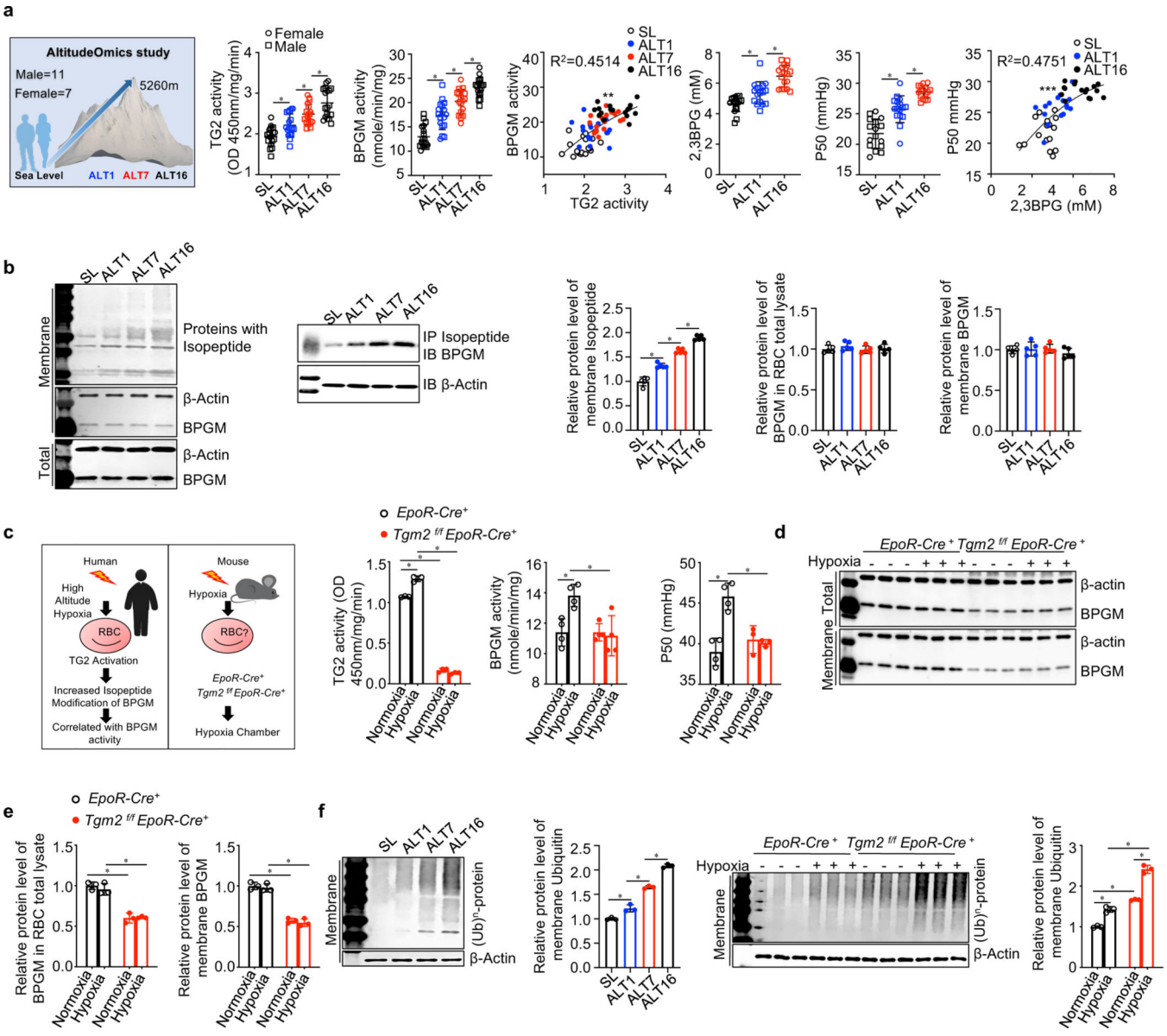

Figure 1. Hypoxia Induces eTG2 activity in both humans and mice.

a. Schematic representation of AltitudeOmics project design; TG2 & BPGM activity, 2,3-BPG and P50 in human erythrocytes at sea level (SL) and at high altitude on day 1 (ALT1), day 7 (ALT7) or day 16 (ALT16). Circles represent females, squares represent males. **P*<0.05, (n=16–18). ***P*<0.05, Pearson correlation analysis, r^2=0.4514. P50 was significantly correlated with 2,3BPG, ****P*<0.05, Pearson correlation analysis, r^2=0.4751.

b. Effect of high-altitude hypoxia on isopeptide modification and BPGM protein levels in human erythrocytes and IP Isopeptide followed by Western blot against BPGM; Protein bands were quantitated and normalized to the sea level. **P*<0.05, (n=5).

c. Experimental design for mouse model of human hypoxia. Erythrocyte BPGM and TG2 activity were quantified in *EpoR-Cre*$^{+}$ mice and *Tgm2*$^{f/f}$*EpoR-Cre*$^{+}$ mice under normoxia and hypoxia (10% O_2 for 48h). **P*<0.05, (n=3 or 4).

d-e. *In vivo* effect of hypoxia exposure on murine erythrocyte BPGM protein level (d). Protein bands were quantified and normalized to the *EpoR-Cre*$^{+}$ mice under normoxia (e). **P*<0.05, (n=3).

f. *In vivo* effect of high altitude hypoxia and hypoxia exposure on proteins modified by ubiquitin in human (left panel) and mouse (right panel) erythrocytes. Protein bands were quantified and normalized to humans at sea level and *EpoR-Cre*$^{+}$ mice under normoxia. **P*<0.05, (n=3). All of data are expressed as mean ± SD. Statistical analyses among SL, ALT1, ALT7 and ALT16 were conducted by one-way ANOVA followed with Sidak's multiple comparisons test. Statistical analyses between *EpoR-Cre*$^{+}$ and *Tgm2*$^{f/f}$*EpoR-Cre*$^{+}$ mice treated with or without Ang II were conducted by two-way ANOVA followed with Sidak's multiple comparisons test. See also Figure S1, Figure S2 and Table S1.

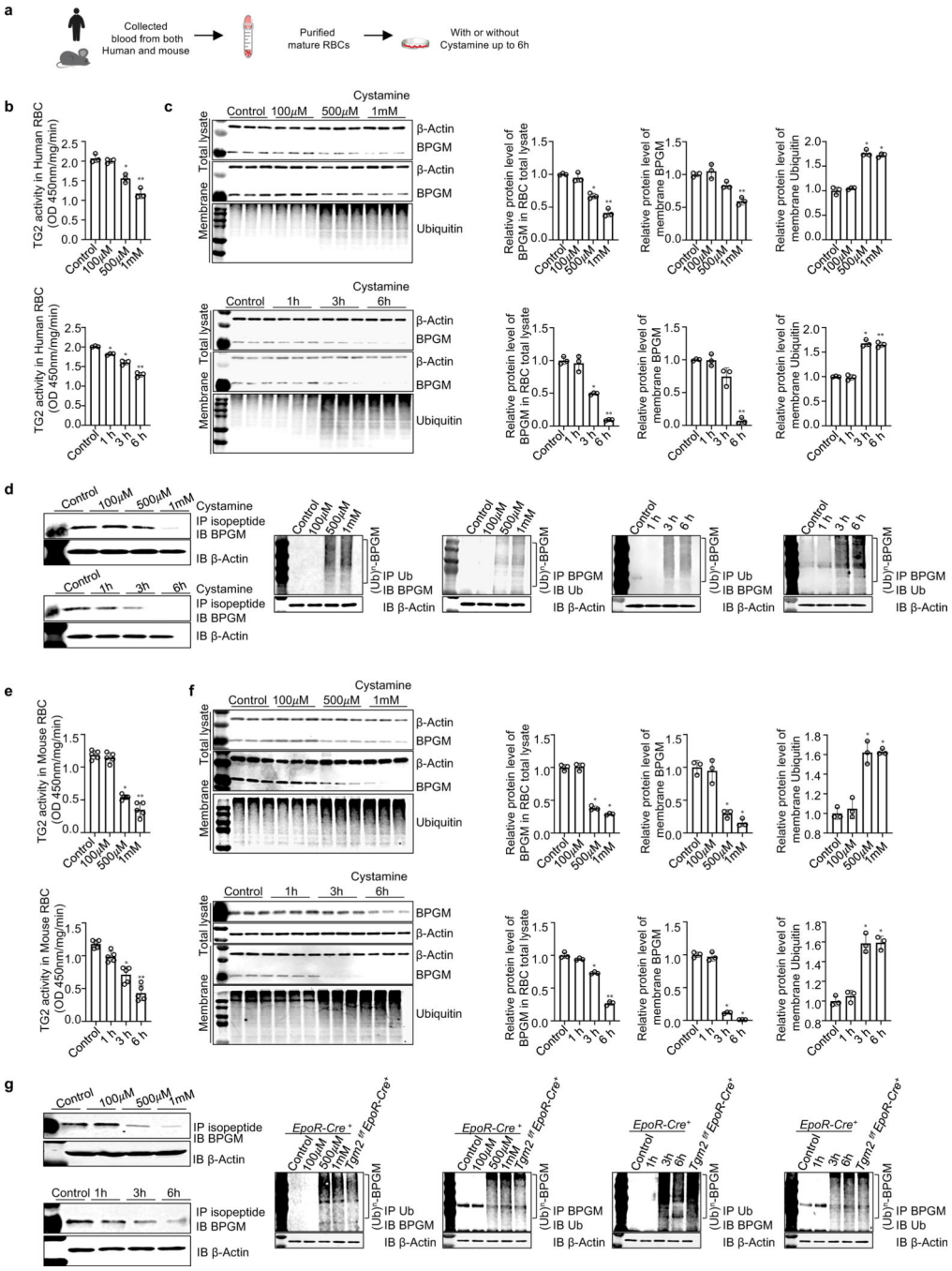

Figure 2. TG2-mediated PTM stabilizes erythrocyte BPGM and maintains protein homeostasis by competing against polyubiquitination and degradation.

a. Schematic representation of experiment design.

b. In human erythrocytes, TG2 activity was reduced by cystamine treatment in a dose (upper panel) and time (lower panel) dependent manner (n=3).

c. *In vitro* inhibitive effect of cystamine on TG2-mediated isopeptide modification on BPGM protein and proteins modified with ubiquitin in cultured human erythrocytes are dose-

dependent (upper panel) and time-dependent (lower panel). Protein bands were normalized to untreated erythrocytes (n=3).

d. Isopeptide modification of BPGM mediated by TG2 was reduced by cystamine treatment in a dose and time dependent manner in cultured human erythrocytes (left panel). IP BPGM followed by western blot against ubiquitin and vice versa (right panels).

e. In mouse erythrocytes, TG2 activity was reduced by cystamine treatment in a dose (upper panel) and time (lower panel) dependent manner (n=5).

f. Effect of cystamine on BPGM protein and proteins modified with ubiquitin in mouse RBCs is in a dose (upper panel) and time (lower panel) dependent manner, followed with quantification of protein bands by densitometry (n=3).

g. IP isopeptide followed by western blot against BPGM; IP BPGM followed by western blot against ubiquitin and vice versa. Data are expressed as mean ± SD. For different dosage treatment, $*P<0.05$ versus control, $**P<0.05$ versus 500 μM. For different time points, $*P<0.05$ versus control, $**P<0.05$ versus 3h. Data were analyzed by one-way ANOVA followed with Sidak's multiple comparisons test. See also Figure S2.

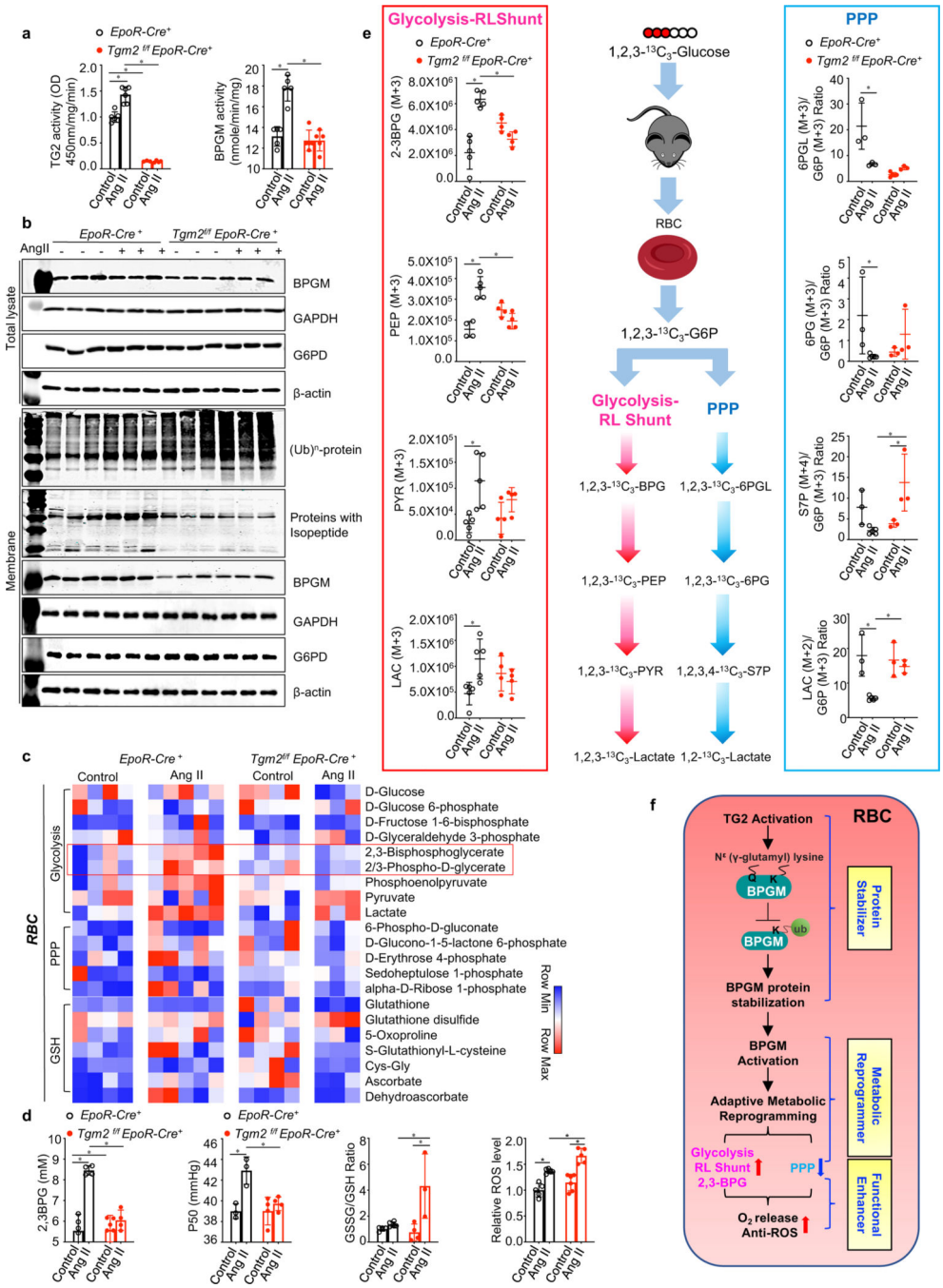

Figure 3. Beneficial role of erythrocyte TG2-mediated BPGM stabilization under pathological hypoxia by promoting erythrocyte adaptive metabolic reprogramming for enhanced O_2 delivery.

a. BPGM activity and TG2 activity in *EpoR-Cre*$^{+}$ and *Tgm2*$^{f/f}$*EpoR-Cre*$^{+}$ mice in Ang II infusion-induced CKD model. **P*<0.05 (n=3–6).

b. Effect of Ang II-mediated pathological hypoxia on the protein levels of BPGM, GAPDH, G6PD, ubiquitin and isopeptide, followed with the quantification of protein bands by densitometry.

c. Heat map of erythrocyte glucose metabolism measured by untargeted metabolomics.

d. Erythrocyte 2,3-BPG levels were measured by commercially available kit. Erythrocyte oxygen release capacity (P50) was measured by a Hemox analyzer. The GSSG/GSH ratio was quantified by untargeted metabolomics. Erythrocyte ROS levels were detetermined by flow cytometry *P<0.05, (n=3–6).

e. *In vivo* flux experiments with $^{13}C_{1,2,3}$-glucose to trace glucose metabolism between Glycolysis-RLShunt and PPP. Isotopically labeled 2,3-BPG (M+3), PEP (M+3), PY(M+3) LAC (M+3), and the ratio of 6PGL (M+3)/G6P (M+3),6PG (M+3)/G6P (M+3), S7P (M+4)/G6P (M+3), LAC (M+2)/G6P (M+3). *P<0.05, (n=3–5).

f. Schematic illustration of eTG2-dependent stabilization of BPGM protein in adaptive metabolic reprogramming and functional regulation in RBC. Data are expressed as mean ± SD and were analyzed by two-way ANOVA followed with Sidak’s multiple comparisons test. See also Figure S3.

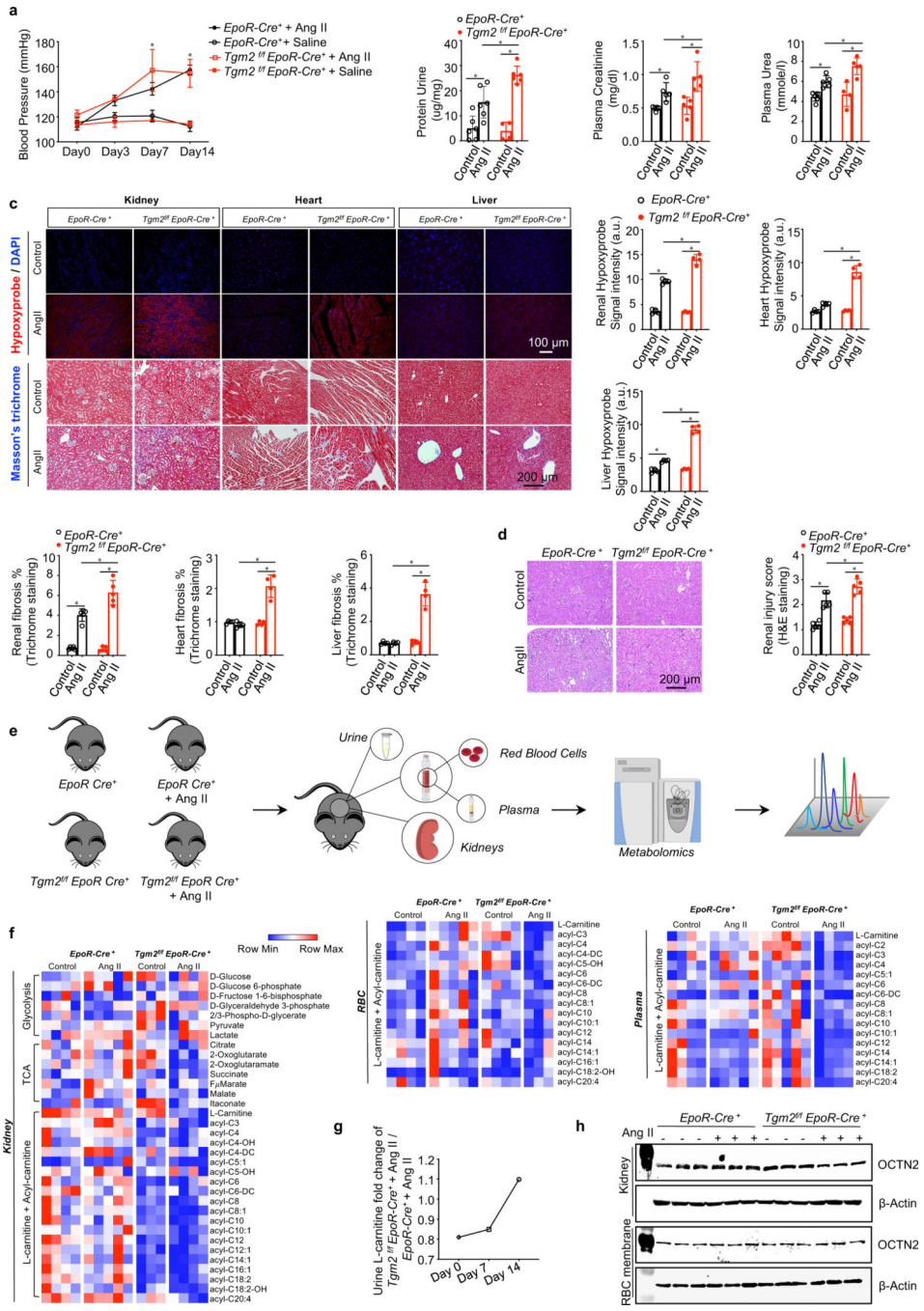

Figure 4. Erythrocyte TG2 deletion exacerbates Ang II-induced CKD manifestations and disturbs L-carnitine-dependent renal metabolism.

a. Systolic blood pressure (BP) was measured on days 0, 3, 7 and 14 of Ang II infusion. **P*<0.05, Saline versus Ang II (n=4–6). kits. **P*<0.05, (n=4–6).

b. Urinary protein, plasma creatinine and plasma urea were quantified by commercially available kits. **P*<0.05, (n=4–6).

c. Top panel: Representative images of hypoxyprobe staining in kidney, heart and liver (scale bar=100 μm). Bottom panels: Representative images of Masson's trichrome staining in kidney,heart and liver (scale bar=200 μm). **P*<0.05 (n=4).

d. Representative hematoxylin and eosin (H&E) staining of sections of kidney cortex (scale bar=200 μm). **P*<0.05, (n=4).

e. Experimental design for mouse sample collection and metabolomics study.

f. Untargeted metabolomics screening data indicated L-carnitine and acyl-carnitine loss in kidney, erythrocyte (RBC) and plasma, (n=3–5).

g. Urine L-carnitine fold change of $Tgm2^{f/f}$ *EpoR-Cre*$^{+}$ + Ang II versus *EpoR-Cre*$^{+}$ mice + Ang II.

h. Protein levels of OCTN2 in kidneys and erythrocyte membranes. All data are expressed as mean ± SD and were analyzed by two-way ANOVA followed with Sidak's multiple comparisons test. See also Figure S4 and Table S2.

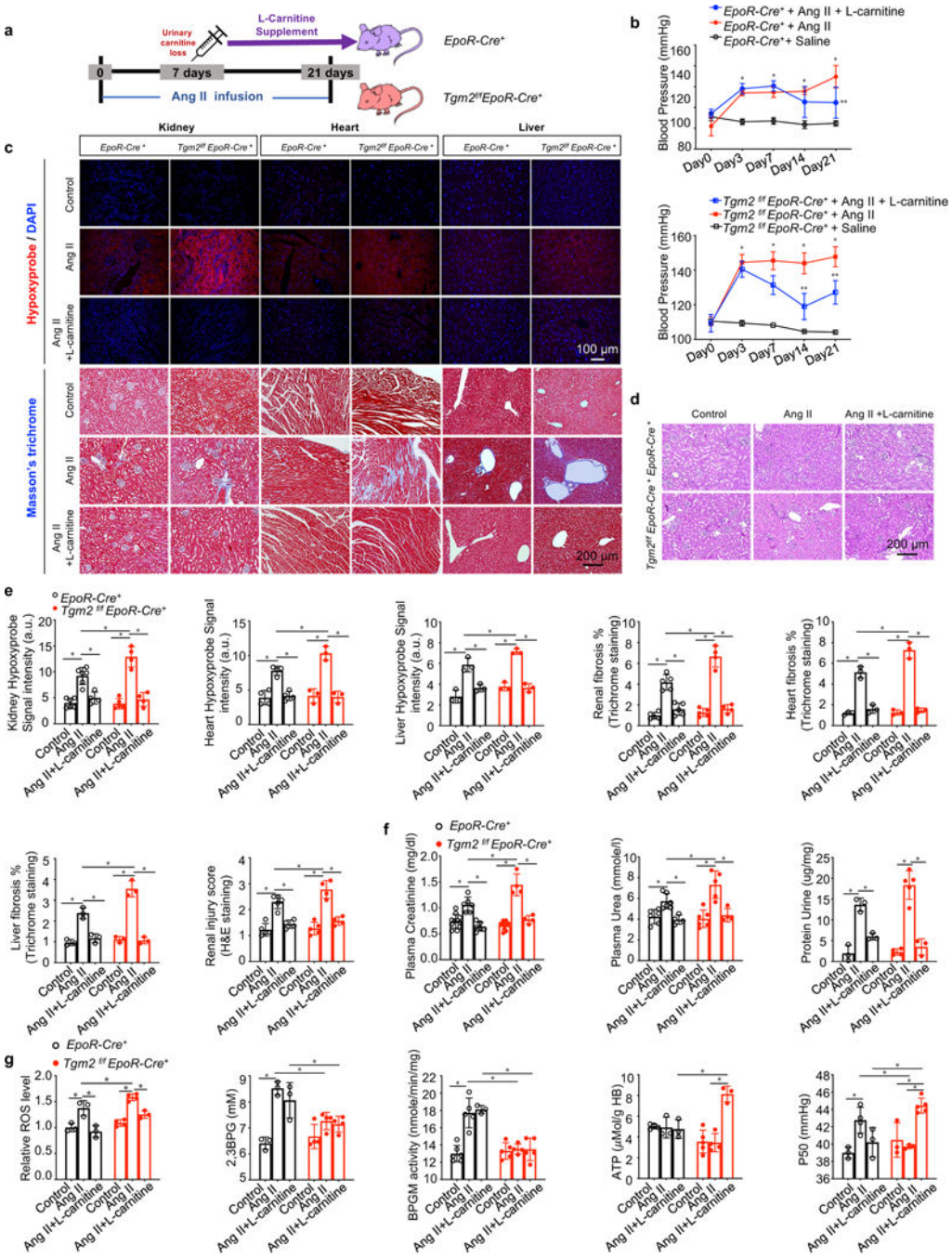

Figure 5. L-carnitine supplementation improves tissue oxygenation and combats progression of CKD.

a. Schematic representation of rescue experiment design. L-carnitine was supplemented from Day 7 to Day 21.

b. Systolic blood pressure (BP) was measured day 0 up to day 21. **P*<0.05, Saline versus Ang II, ***P*<0.05, AngII versus Ang II+ L-carnitine, (n=3–5).

c. Top panel: Representative images of hypoxyprobe staining in kidney, heart and liver (scale bar=100 μm). Bottom panels: Representative images of Masson's trichrome staining in kidney, heart and liver (scale bar=200 μm).

d. Representative hematoxylin and eosin (H&E) stained kidney sections are shown (scalebar=200 μm).

e. Statistical analysis of Hypoxyprobe staining, Masson's trichrome staining (kidney, heart and liver) and renal injury score. *P<0.05 (n=3–6). kits. *P<0.05 (n=3–11).

f. Urinary protein, plasma urea and plasma creatinine were quantified by commercially available kits. *P<0.05 (n=3–11).

g. Relative ROS levels were determined by flow cytometry. 2,3-BPG levels, BPGM activity and ATP levels were measured by commercially available kits. Erythrocyte oxygen release capacity (P50) was measured by a Hemox analyzer. *P<0.05 (n=3–5). All data are expressed as mean ± SD and were analyzed by two-way ANOVA followed with Sidak's multiple comparisons test.

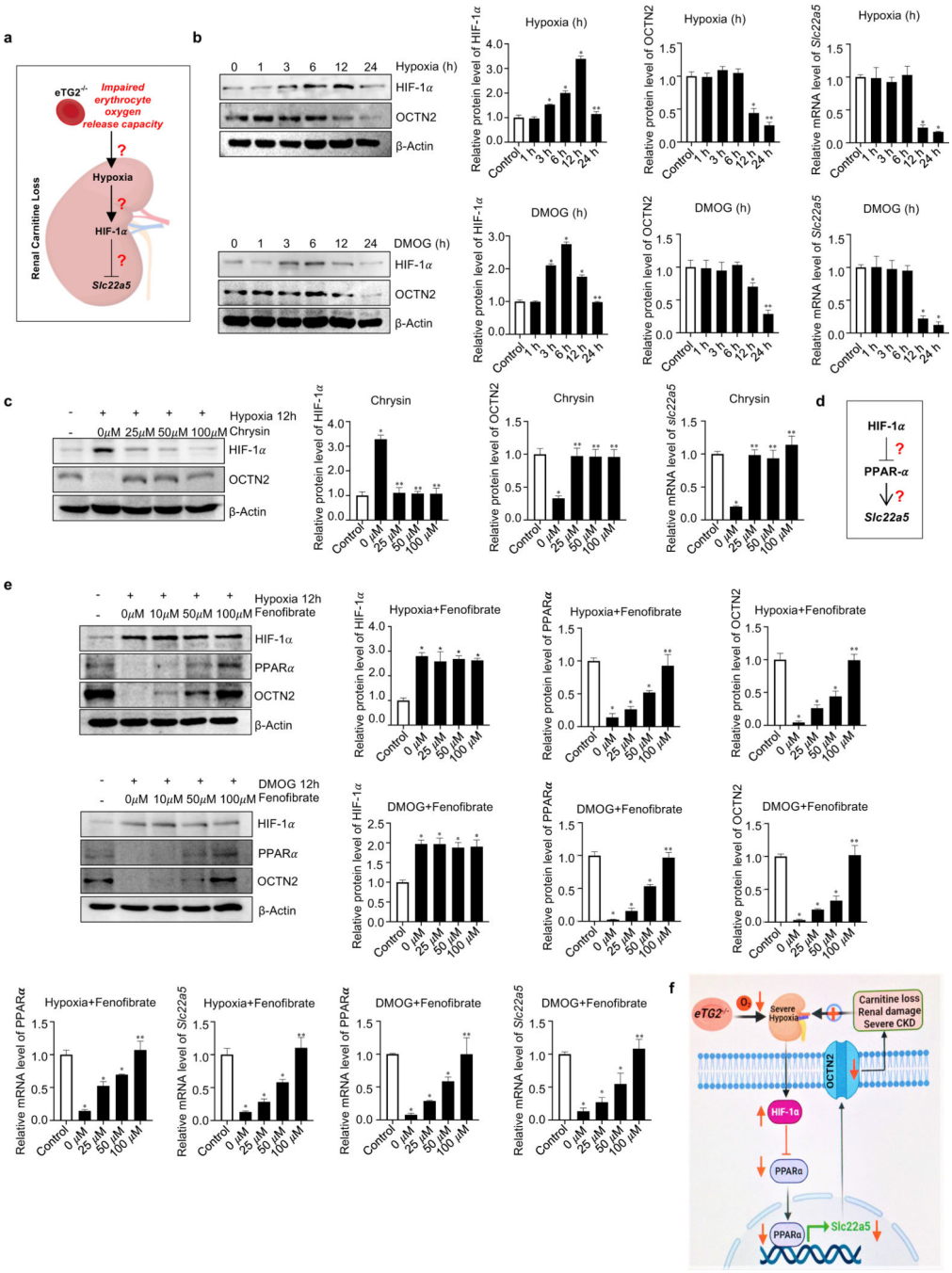

Figure 6. Hypoxia-mediated downregulation of OCTN2 via HIF-1α-PPARα axis is a key molecular mechanism linking eTG2 ablation to Ang II-induced carnitine loss, renal damage and severe CKD.

a. Schematic hypothesis linking renal hypoxia with HIF-1α induction and reduced *Slc22a5* transcription.

b. Hypoxia (1% O_2, upper panel) or DMOG (1mM, lower panel) treatment directly induced HIF1-α and reduced OCTN2 protein levels in a time-dependent manner in cultured murine kidney explants. Protein bands were normalized to control group. qRT-PCR analyses of

Slc22a5 mRNA levels in kidney samples from the same treatment was followed with protein quantification. **P*<0.05 versus Control, ***P*<0.05 versus 12h, (n=3).

c. Induction of HIF-1α and reduction of OCTN2 protein levels and *Slc22a5* mRNA levels were attenuated by Chrysin treatment in cultured murine renal explants. **P*<0.05 versus Control, ***P*<0.05 versus 0 μM Chrysin, (n=3).

d. Hypothesis that PPARα functions downstream of HIF-1α underlying hypoxia-mediated reduction in *Slc22a5* transcription.

e. Fenofibrate, a PPARα agonist, restored hypoxia (upper panel) or DMOG-mediated (lower panel) reduction of OCTN2 and PPARα proteins and their mRNA levels in a dosage-dependent manner in cultured mouse kidney explants. **P*<0.05 versus Control, ***P*<0.05 versus 50 μM Fenofibrate, (n=3).

f. Signaling pathways linking eTG2 deficiency to renal damage and CKD: Decreased erythrocyte O_2 offload in *eTG2*$^{-/-}$ mice leads to renal hypoxia and reduction of renal *Slc22a5* transcription and decreased OCTN2 via HIF1α-PPARα axis. Without intervention, renal hypoxia, reduced OCTN2 levels and carnitine loss function as a malicious positive feed forward loop to promote severe hypoxia, excess carnitine losses, renal damage and severe CKD progression. All data are expressed as mean ± SD and were analyzed by two-way ANOVA followed with Tukey's multiple comparisons test.

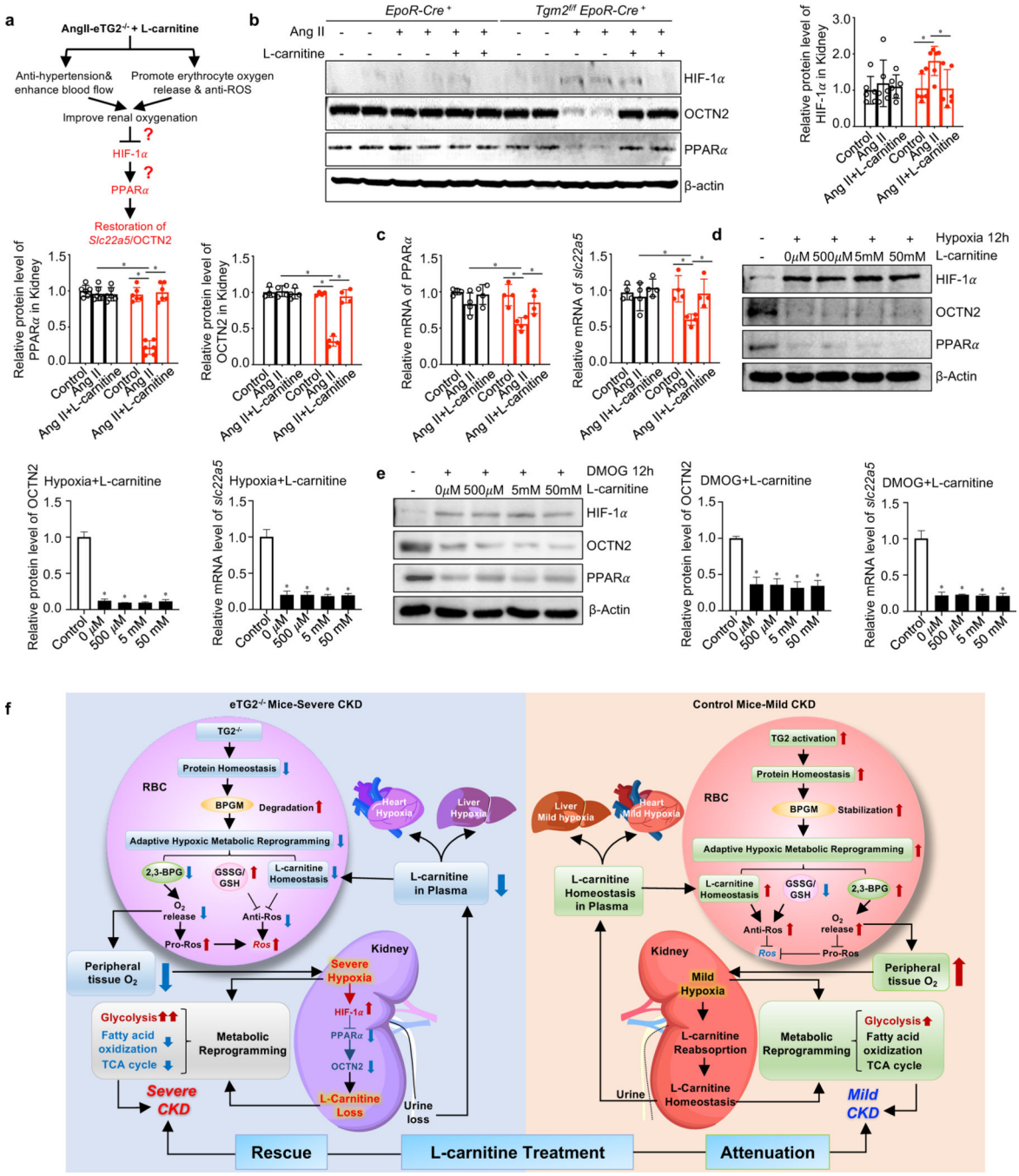

Figure 7. Restoration of renal OCTN2 underlies the improvement in CKD by carnitine supplementation in Ang II-infused *eTG2*$^{-/-}$ mice

a. Hypothesis: L-carnitine supplementation has dual therapeutic effects to lower renal hypoxia including reducing hypertension and increasing O_2 offload.

b. Protein levels of HIF-1α, OCTN2 and PPARα were detected by Western blot in kidney tissues from *EpoR-Cre*$^{+}$ and *Tgm2*$^{f/f}$*EpoR-Cre*$^{+}$ mice with or without L-carnitine treatment. Protein bands were normalized to the control group. $^{*}P < 0.05$, (n=4–6).

c. qRT-PCR analyses of *Slc22a5* and PPARα mRNA levels from the same groups in b. **P* < 0.05, n=4.

d-e. The protein levels of HIF-1α, OCTN2 and PPARα and the mRNA levels of *Slc22a5* in isolated kidney organ cultures were detected after hypoxia (d) or DMOG (e) in the presence or absence of various dosages of L-carnitine. **P* < 0.05, n=3.

f. Working model: eTG2 deletion impairs protein homeostasis, leading to BPGM protein degradation, in turn impairing adaptive hypoxic metabolic reprograming in erythrocytes and peripheral tissues. As for erythrocytes, decreased adaptive hypoxic metabolic reprograming is associated with reduced L-carnitine and acyl-carnitine, increased GSSG/GSH ratio and reduced 2,3-BPG production, all of which contributes to intracellular ROS increase. As for kidneys, both hypoxia and L-carnitine loss led to impaired adaptive hypoxic metabolic reprograming, increased glycolysis, reduced fatty acid oxidation and TCA activity. Hypoxia-mediated downregulation of OCTN2 via HIF-1α-PPARα axis is a key molecular link of eTG2 ablation to Ang II-induced carnitine loss, renal damage and severe CKD. As for heart and liver, insufficient L-carnitine and oxygen adaptive hypoxic metabolic reprograming leads to fibrosis. L-carnitine supplementation exhibited dual therapeutic effects including reduced hypertension and increased O_2 delivery and reduced ROS in erythrocytes in eTG2$^{-/-}$ mice. As such, improved renal oxygenation restores renal HIF-1α-PPAR α-OCTN2 levels, maintains carnitine homeostasis and rescues severe CKD phenotype in eTG2-deficient mice. In control mice, eTG2-depedent O_2 delivery is enhanced. Thus, L-carnitine attenuates mild CKD phenotype with dual therapeutic effects including reduced hypertension and lowered ROS in erythrocytes. All data are expressed as mean ± SD and were analyzed by two-way ANOVA followed with Sidak's multiple comparisons test. See also Figure S5.

Key resources table

REAGENT or RESOURCE	SOURCE	IDENTIFIER
Antibodies		
Rabbit polyclonal to Solute carrier family 22 member 5 (OCTN2)	Abcam	Cat# ab180757; RRID:AB_2751018
Rabbit polyclonal Transglutaminase 2 antibody	GeneTex	Cat# GTX111702; RRID:AB_1952227
Rabbit polyclonal BPGM antibody	Proteintech	Cat# 17173-1-AP; RRID:AB_2274991
Rabbit polyclonal GAPDH antibody	Invitrogen	Cat# PA1-987; RRID:AB_2107311
Mouse monoclonal [81D1C2] to Isopeptide	Abcam	Cat# ab422; RRID:AB_304383
Mouse monoclonal antibody to Ubiquitin (P4D1)	Santa Cruz	Cat# sc-8017; RRID:AB_2762364
Rabbit polyclonal PPAR alpha antibody	Invitrogen	Cat# PA585125; RRID:AB_2792272
Rabbit polyclonal HIF1A antibody	Invitrogen	Cat# PA1-16601; RRID:AB_2117128
Mouse monoclonal β-Actin (8H10D10) antibody	Cell Signaling Technology	Cat# 3700S; RRID:AB_2242334
IRDye 800CW Donkey anti-Rabbit IgG	LI-COR	Cat# 926-32213; RRID:AB_621848
IRDye 680RD Donkey anti-Mouse IgG	LI-COR	Cat# 926-68072; RRID:AB_10953628
Biological samples		
Human RBC sample	University of Colorado School of Medicine	AltitudeOmics project
Chemicals, peptides, and recombinant proteins		
Cystamine	Sigma	Cat# 30050
DMOG	Selleckchem	Cat# S7483
Chrysin	Selleckchem	Cat# S2281
Fenofibrate	Selleckchem	Cat# S1794
L-carnitine	Selleckchem	Cat# S2388
Beads conjugated with anti-ε-(γ-glutamyl)-lysine isopeptide IgM (81D4)	Covalab	Cat# opr0003
protease inhibitor cocktail	Roche	Cat# 11697498001
phosphatase inhibitor cocktail	Roche	Cat# 04906837001
proteasome inhibitor MG132	Santa Cruz	Cat# sc-201270
Bortezomib	Santa Cruz	Cat# sc-217785
CM-H2DCFDA	Invitrogen	Cat# C6827
Percoll	GE Healthcare Life Sciences	Cat# 17-5445-01
Protein G Sepharose beads	GE Healthcare Life Sciences	Cat# 17-0618-01
D-Glucose-1,2,3-$^{13}C_3$	Sigma-aldrich	Cat# 720127
Angiotensin II	Sigma-aldrich	Cat# A9525
Critical commercial assays		
Creatinine colorimetric assay kit	Abcam	Cat# ab65340

REAGENT or RESOURCE	SOURCE	IDENTIFIER
Urea assay kit	Sigma-Aldrich	Cat# MAK006
Mouse Albumin ELISA Assay kit	Exocell	Cat# 1011
Creatinine Chemical Assay Kit	Exocell	Cat# 1012
ATP Colorimetric/Fluorometric Assay Kit	BioVision	Cat# K354-100
2,3-Diphosphoglycerate (2,3-DPG)	Roche	Cat# 10148334001
Transglutaminase Assay Kit	Sigma-Aldrich	Cat# CS1070
Hypoxyprobe Omni Kit	Hypoxyprobe	Cat# HP3-200 Kit
Deposited data		
Metabolic screening-RBC	This paper	Supplementary Data1
Metabolic screening-Kidney	This paper	Supplementary Data2
Metabolic screening-Plasma	This paper	Supplementary Data3
Metabolic screening-Urine	This paper	Supplementary Data4
Experimental models: Organisms/strains		
EpoR-Cre^{+} mice	Stuart H. Orkin	MGI: 3052727
Tgm2$^{flox/flox}$ mice	University of Rochester, New York	N/A
C57BL/6 mice	Jackson Laboratory	Stock No:000664
Oligonucleotides		
Primers for RT-PCR, see Table S2	This paper	N/A
Primers for genotyping *EpoR-Cre*$^{+}$: GTGTGGCTGCCCCTTCTGCCA, CAGGAATTCAAGCTCAACCTCA	This paper	N/A
Primers for genotyping *Tgm2*$^{flox/flox}$: GGCAAGGTCTGAGAAAGCAC, CACGTAGACTGTTCCCAGCA	This paper	N/A
Software and algorithms		
BD FacsDiva software	BD Biosciences	version 6.2
Image-J software	National Institutes of Health	https://imagej.nih.gov/ij/
Graphpad Prism	Graphpad Prism (version 8.3.1)	https://www.graphpad.com/scientific-software/prism/
Scaffold	Proteome Software	version 4.8